Sensors and Actuators Reports 3 (2021) 100041

Contents lists available at ScienceDirect

Sensors and Actuators Reports

journal homepage: www.elsevier.com/locate/snr

Surface acoustic waves in biosensing applications

Yuqi Huang, Pradipta Kr. Das, Venkat R. Bhethanabotla *

Department of Chemical and Biomedical Engineering, University of South Florida, Tampa, FL 33620-5350, USA

ARTICLE INFO

Keywords:
Surface acoustic waves
Biosensor
Non-specific binding removal
Acoustic streaming

ABSTRACT

In this paper, we review the utilization of surface acoustic waves in biosensing applications. A brief background on the theoretical aspects and on the modeling principles for acoustic wave propagation in a liquid medium is provided first. Subsequently, different types of surface acoustic waves (SAWs) generated on piezoelectric substrates are discussed, with the basics of wave formation, operation principles, and material considerations. Several advancements in SAW biosensor design that have been developed to achieve enhanced sensor functionality are also presented. We have overviewed different sensing capabilities of SAW devices in different biosensing applications, such as the detection and manipulation of cells, and the quantification on proteins, vapor molecules and DNA hybridizations. The challenge of biofouling, which can affect the sensitivity and specificity of bioassays, is addressed in detail. Several techniques used to reduce biofouling are discussed including one based on acoustic streaming using Rayleigh SAWs. With their ability to mitigate sensor signal interference due to biofouling, and reduce incubation times using acoustic streaming, and combined with their high sensitivity, SAWs can be used as cost-effective platforms for various point of need (PON) based biosensing applications.

1. Introduction

A biosensor is a device that can detect a biologically-active analyte, such as a biomolecule, a biochemical structure, or a macromolecule, utilizing a physiochemical transducer. The data can be collected by converting the biological recognition event into a usable output signal [1,2]. Sensing systems have been constructed for a variety of biological components, including enzymes, antibodies, antigens, nucleic acids, isolated receptors, whole cells, microorganisms, and plant and animal tissues [3]. A key feature of a successful biosensor is the selectivity of the recognition element for a given target in the presence of other potentially interfering matrix elements [2]. The ability to detect the presence or measure the concentration of biomolecules with high sensitivity will facilitate the diagnosis and monitoring of various diseases [4]. Successful biosensor development entails meeting several key goals: (1) The biosensor should be low-cost; (2) The test should involve limited pretreatment of the sample; (3) The test shouldn't require large sample volumes; and (4) The biosensor can be used by personnel with limited technical skill. Biofouling from non-specifically bound (NSB) proteins and slow incubation times are significant factors that must be addressed to attain these goals and construct compact, low-cost point of need (PON) biosensing systems and platforms that are both selective and sensitive.

Acoustic wave devices that have been used for sensing applications and materials characterization include thickness shear mode (TSM) resonators [5], surface acoustic wave (SAW) devices [6], acoustic plate mode devices (APM) [7] and flexural plate wave (FPW) [8] devices. In one-port acoustic devices such as TSM, a single port serves as both the input and the output terminals, whereas in two-port devices such as SAW, APM and FPW, one port is used for input and the other is used for output. The input signal generates an acoustic wave that propagates to a receiving transducer which then regenerates an electrical signal at the output port. The sensor response is determined based on the relative signal levels and phase delay between the input and the output ports.

This review gives a brief overview of several different acoustic wave devices used as biosensors, presents background on various surface waves generated on piezoelectric substrates, and surveys the field of surface acoustic wave biosensors [9] through an explanation of operation principles, design considerations and a summary of recent experimental applications. An overview of the various theoretical approaches that have been utilized to model sensor response and wave propagation characteristics in acoustic wave devices is also presented. SAW-based biosensors have great potential in PON biological testing [10]. They can provide the high sensitivity required for medical diagnostics and can be configured to mitigate interference from non-specifically bound (NSB) proteins and reduce incubation times to clinically-expedient levels for compact yet selective PON platforms. The NSB removal and mixing capabilities facilitated by acoustic streaming from SAWs can be combined with other detection and analyte quantification modalities such as fluorescence, SPR, and electrochemical to advance a number of biosensing platforms. With development of compact and inexpensive SAW-based biosensors, platforms that can quantify biomarkers such as proteins from real matrices such as blood and urine at PON are possible

* Corresponding author.
E-mail address: bhethana@usf.edu (V.R. Bhethanabotla).

https://doi.org/10.1016/j.snr.2021.100041
Received 13 December 2020; Revised 2 April 2021; Accepted 2 April 2021
Available online 10 April 2021

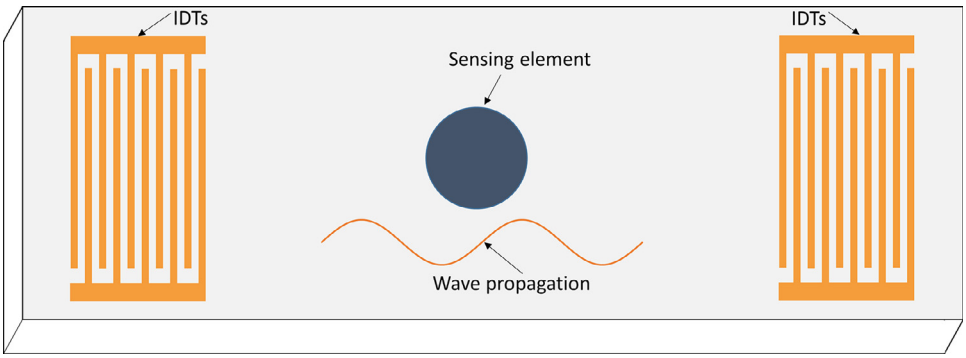

Fig. 1. Schematic illustration of a delay-line SAW device with interdigital transducers (IDTs) fabricated on a piezoelectric substrate. Sensing element is placed on the delay line path.

[10]. In this review, we provide a complete discussion of how surface acoustic waves may be utilized in such biosensor platforms.

2. Theoretical aspects of acoustic wave biosensors

2.1. Piezoelectricity

Acoustic waves are generated in several anisotropic materials which convert electric signals to mechanical motion and *vice versa*. These materials are said to be 'piezoelectric', an effect which was first described by Pierre and Paul-Jacques Curie in the late 19th century [11]. The constitutive equations for piezoelectric materials are given by [12–14]

$$T_{ij} = c_{ijkl}S_{kl} - \mathrm{e_{kij}E_k} \tag{1a}$$

$$D_i = e_{ikl}S_{kl} + \varepsilon_{ik}E_k \tag{1b}$$

Here, T_{ij}, D_i, c_{ijkl}, S_{kl}, e_{kij}, E_k, ε_{ik} represent stress components, electric displacement, elastic moduli at constant electric field, strain tensor components, the piezoelectric constant, electric field, and permittivity at constant strain, respectively. The equation of motion in the absence of any body force is given by [12,13]:

$$\frac{\partial T_{ij}}{\partial x_j} - \rho\frac{\partial^2 \mathrm{u_i}}{\partial \mathrm{t}^2} = 0 \tag{2a}$$

$$\frac{\partial D_i}{\partial x_i} = 0 \tag{2b}$$

where ρ and u_i represent mass density and the solid displacement components, respectively. Note that the strain tensor can be correlated to solid displacement fields as

$$S_{kl} = \frac{1}{2}\left(\frac{\partial u_k}{\partial x_l} + \frac{\partial u_l}{\partial x_k}\right) \tag{3}$$

To efficiently convert the electrical signal to an acoustic one, interdigital transducers (IDTs) are fabricated on the surface of the piezoelectric substrate as shown in Fig. 1. When the IDTs are excited via an electrical signal, surface acoustic waves (SAWs) are generated for which displacement and amplitude depend upon input electric power, frequency, and material.

The structure of the IDTs also plays a significant role in determining the directionality and frequency of the resultant SAWs. In order to generate focused SAWs, concentric IDTs are fabricated to concentrate acoustic energy to a focal point. Sankaranarayanan and Bhethanabotla [15] carried out numerical simulations for F-SAW device and demonstrated the concentric propagation of SAW energy to the focal point (Fig 2). They also calculated the insertion loss as a function of SAW frequency for different degrees of arc. It should be noted here that minimizing insertion loss for a given IDT arrangement is important as it maximizes the utilization of SAW energy [16–18].

The use of a SAW device for biosensing applications mostly revolve around measuring its response to mechanical or electrical perturbations. The phase velocity of surface acoustic waves strongly depends on changes in mass loading (Δm), electrical signals (Δe_s) and mechanical parameters (ΔM). The change in phase velocity (ΔV) in terms of external

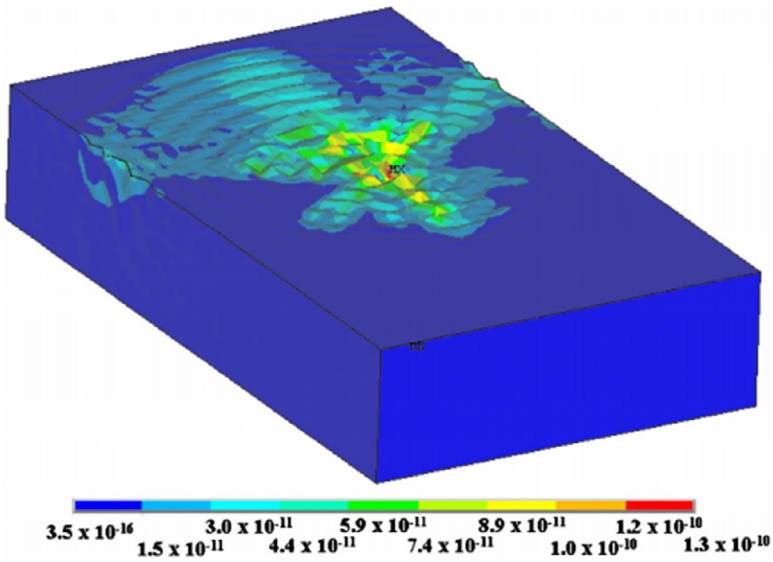

Fig. 2. Simulated acoustic wave propagation in a focused SAW device. Parameters are: F-IDTs having degree of arc $D_a = 120°$, geometric focal length $f_L = 85$ μm, and wavelength $\lambda = 40$ μm. Reproduced with permission [15].

perturbations can be expressed as

$$\Delta V = \frac{\partial V}{\partial m}\Delta m + \frac{\partial V}{\partial e_s}\Delta e_s + \frac{\partial V}{\partial M}\Delta M \tag{4}$$

A number of perturbation parameters such as mass loading, viscosity, and electric and dielectric properties at the interface determine wave/matter interactions [19]. Propagation of an acoustic wave through a piezoelectric material causes a layer of bound charges to form at the surface. The bound charges induce an electric field that moves charge carriers and dipoles in a medium adjacent to the surface. As a result, energy from the propagating wave is removed, altering velocity and attenuation. This is called the acoustoelectric effect [20]. Metallizing the sensing area has been found to efficiently eliminate acoustoelectric effects.

2.2. Acoustic streaming

When a fluid sample is placed on the delay path of a SAW device, the acoustic wave comes into contact with the fluid and is refracted into it due to the difference in sonic velocity in the fluid (c_f) and the piezoelectric material (c_s), with the angle of refraction given by $\theta = \sin^{-1}(c_f/c_s)$. The propagation of acoustic waves into the fluid generates an oscillatory flow in addition to a mean flow known as acoustic streaming [21–23]. Acoustic streaming finds numerous applications in biosensing and hence we present a theoretical description of the phenomenon here. The equations governing continuity, momentum, and energy for a Newtonian fluid are given by

$$\frac{\partial \rho_f}{\partial t} + \nabla.(\rho_f \mathbf{v}) = 0 \tag{5}$$

$$\frac{\partial}{\partial t}(\rho_f \mathbf{v}) = \nabla.\left[\sigma - p\mathbf{I} - \rho_f \mathbf{v}\mathbf{v}\right] \tag{6}$$

$$\frac{\partial}{\partial t}\left(\rho_f E + \frac{1}{2}\rho_f v^2\right) = \nabla.\left[\mathbf{v}.\sigma - p\mathbf{v} + k\nabla T - \rho_f\left(E + \frac{1}{2}v^2\right)\mathbf{v}\right] \tag{7}$$

where $\mathbf{v}$, ρ_f, E and k are velocity, density, energy, and thermal conductivity of the fluids, respectively; and pressure p is related to density as $p = {c_f}^2\rho_f$. The stress tensor is defined as

$$\sigma = \mu\left[\nabla\mathbf{v} + (\nabla\mathbf{v})^T\right] + \left(\mu_b - \frac{2}{3}\mu\right)[\nabla.\mathbf{v}]\mathbf{I} \tag{8}$$

where μ and μ_b represent dynamic viscosity and bulk viscosity, respectively. The resultant fluid motion can be characterized by two distinct timescales [22,24,25]: (a) a fast timescale on which oscillatory flow (timescale on the order of the oscillation time period) may be visible and (b) a slow timescale on which mean flow (timescale on the order of inertia) may be visible. Based on asymptotic expansion techniques, the pressure and flow fields are expressed as

$$\mathbf{v} = \varepsilon\mathbf{v}_1 + \varepsilon^2\mathbf{v}_2 + O(\varepsilon^3) \tag{9a}$$

$$\rho_f = \rho_{f0} + \varepsilon\rho_{f1} + \varepsilon^2\rho_{f2} + O(\varepsilon^3) \tag{9b}$$

$$p = p_0 + \varepsilon p_1 + \varepsilon^2 p_2 + O(\varepsilon^3) \tag{9c}$$

$$E = E_0 + \varepsilon E_1 + \varepsilon^2 E_2 + O(\varepsilon^3) \tag{9d}$$

$$T = T_0 + \varepsilon T_1 + \varepsilon^2 T_2 + O(\varepsilon^3) \tag{9e}$$

Here, the fluid velocity before acoustic excitation has been assumed to be zero i.e. $\mathbf{v}_0 = 0$. Note that the above asymptotic expansions are applicable for subsonic applications only where acoustic Mach number $\varepsilon \ll 1$. In most biomedical and microfluidic applications, acoustic Mach number is very small [26–28] and the perturbation-based approach works well for quantifying acoustic streaming effects. After replacing these expressions in the governing equations and using thermodynamic relationships, the resultant first order equations i.e. Eqs. (10–12) can describe the oscillatory flow field pertaining to the fast timescale.

$$\alpha_{p0}\partial_t T_1 - \kappa_{T0}\partial_t p_1 = \nabla.\mathbf{v}_1 \tag{10}$$

$$\rho_{f0}\frac{\partial \mathbf{v}_1}{\partial t} = \nabla.[\sigma_1 - p_1\mathbf{I}] \tag{11}$$

$$\rho_0 c_{p0}\partial_t T_1 - \alpha_{p0} T_0 \partial_t p_1 = k_0\nabla^2 T_1 \tag{12}$$

In the above equations, α_p, κ_T, and c_p denote isobaric thermal expansion coefficient, isothermal compressibility, and heat capacity, respectively. The subscript 0 indicates properties prior to excitation. To account for mean flow corresponding to the slow timescale, the second order equations are expressed in time-averaged form as follows:

$$\rho_{f0}\nabla.\mathbf{v}_2 + \nabla.\langle \rho_{f1}\mathbf{v}_1 \rangle = 0 \tag{13}$$

$$\nabla.\left[\sigma_2 - p_2\mathbf{I} - \rho_{f0}\langle \mathbf{v}_1\mathbf{v}_1 \rangle\right] = 0 \tag{14}$$

$$\nabla.\left[\langle \mathbf{v}_1.\sigma_1 \rangle - \left(1 - \alpha_{p0}T_0\right)\langle p_1\mathbf{v}_1 \rangle + k_0\nabla T_2 + \langle k_1\nabla T_1 \rangle - \rho_{f0}c_{p0}\langle T_1\mathbf{v}_1 \rangle\right] = 0 \tag{15}$$

where $\langle . \rangle$ denotes the time average of any component over one oscillation period. The mean flow and pressure fields obtained by solving Eqs. (13–15) in conjunction with Eqs. (10–12) can be used to calculate the acoustic radiation force and the acoustic force density, which find various applications in particle manipulation, cell sorting, and nonspecifically-bound biofouling removal applications.

2.3. Acoustic force density and acoustic radiation force

The interaction of acoustic waves with the fluid is a non-linear phenomenon which generates a body force called the acoustic body force. This acoustic body force per unit of fluid volume can be obtained from the second order momentum equation, i.e. Eq. (14), and is given by

$$\mathbf{f}_{ac} = -\nabla\left[\langle p_2 \rangle\mathbf{I} + \langle \rho_{f0}\mathbf{v}_1\mathbf{v}_1 \rangle\right] \tag{16}$$

This acoustic body force drives the fluid to undergo mean flow which occurs over slow timescales. This mean flow is used in biomedical applications to manipulate particles and sort cells. To understand the particle motion, we need to estimate the acoustic radiation force acting on small particles where particle radius a is much smaller than the acoustic wavelength (λ). In this scenario, the particle will act as a weak scatterer. Employing first-order scattering theory, the first order velocity field can be decomposed as $\mathbf{v}_1 = \mathbf{v}_{in} + \mathbf{v}_{sc}$ where $\mathbf{v}_{in}$ is the velocity of the incoming wave and $\mathbf{v}_{sc}$ that of the scattered wave propagating away from the particle. The acoustic radiation force can be calculated as the time-averaged force acting on the particle surface Ω and can be expressed as [29]

$$\mathbf{F}_{rad} = -\int_{\Omega}\left[\langle p_2 \rangle\mathbf{n} + \rho_{f0}\langle (\mathbf{n}.\mathbf{v}_1)\mathbf{v}_1 \rangle\right] \tag{17}$$

Note that the above expression is derived for inviscid flow;modeling a viscous layer around the particle has a negligible impact on the acoustic radiation force. For incompressible particles, the first expression of acoustic radiation force was obtained by King [30] and later, Yosika, which Kawasima extended for a compressible particle [31]. In a subsequent study, Gorkov [32] generalized the expression and derived the acoustic radiation force for a spherical particle as

$$\mathbf{F}_{rad} = -2\pi a^3\rho_{f0}\nabla\left(\frac{1}{3}\frac{\langle p_1 p_1 \rangle}{{\rho_{f0}}^2{c_f}^2}f_0 - \frac{1}{2}\langle \mathbf{v}_1\mathbf{v}_1 \rangle f_1\right) \tag{18}$$

where $f_0 = 1 - \frac{\kappa_p}{\kappa_f}$ and $f_1 = \frac{2(\rho_p - \rho_{f0})}{2\rho_p + \rho_{f0}}$; κ_p and κ_f are the compressibilities of the particle and the fluid, respectively; and ρ_p is the density of the particle. Since the acoustic streaming generated in microfluidics is in Stokes flow regime, we can calculate the drag force acting on the particle as $\mathbf{F}_{drag} = 6\pi\mu a(\langle \mathbf{v}_2 \rangle - \mathbf{v}_p)$ where $\mathbf{v}_p$ is the particle velocity. The motion of the particle is therefore given by $\frac{4\pi a^3\rho_p}{3}\frac{d\mathbf{v}_p}{dt} = \mathbf{F}_{drag} + \mathbf{F}_{rad}$.

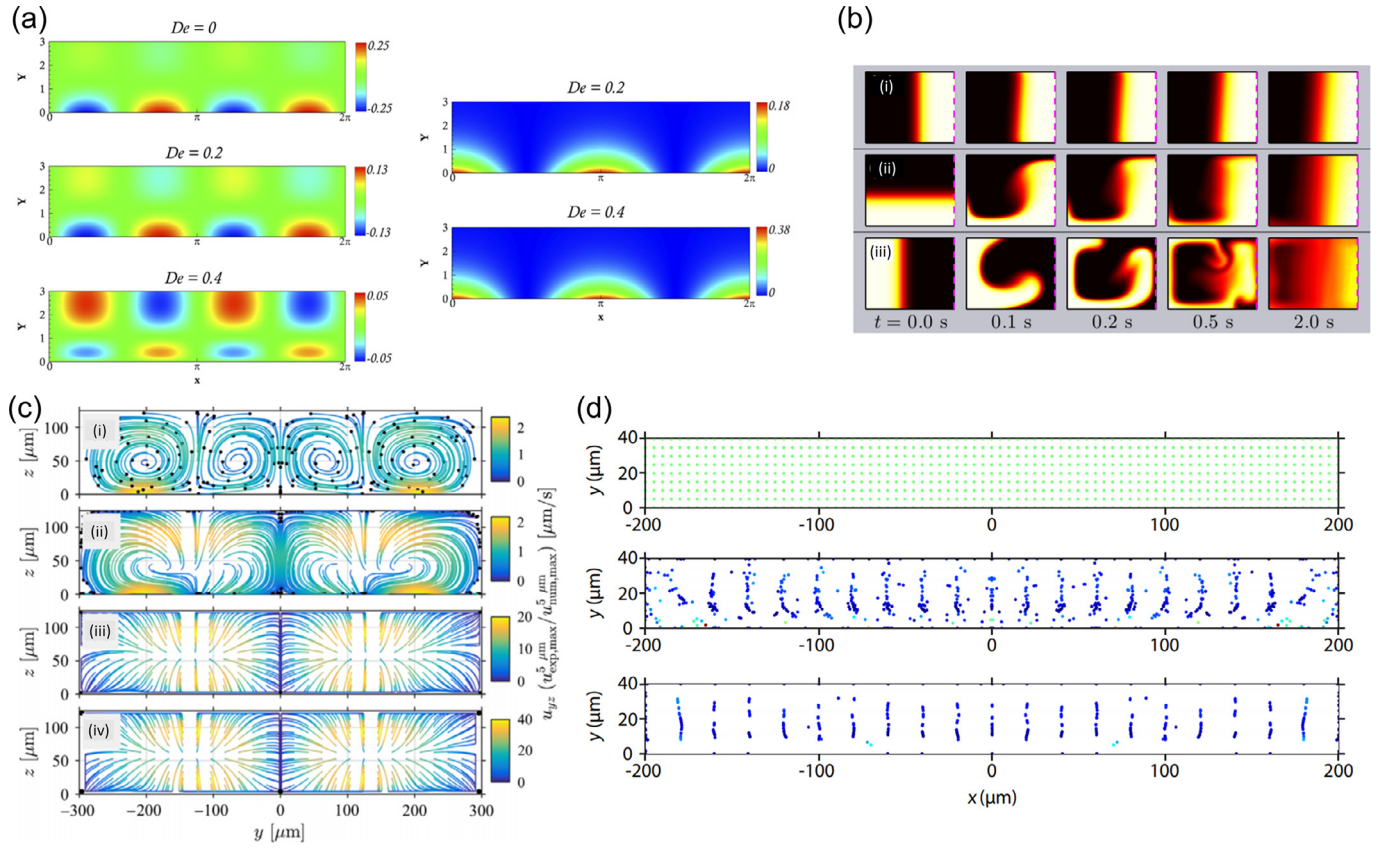

Fig. 3. (a) Surface plot of acoustic force density for a vibrating boundary scenario [23]. Left and right figures show x- and y-components of acoustic force density, respectively. (b) Time evolution of the iodixanol concentration profile in the vertical y-z plane symmetric around y = 0. The results are shown for three different initial configurations: (i) A vertical slab of the dense fluid in the center, (ii) A horizontal slab of the dense fluid at the bottom, and (iii) Two vertical slabs of the dense fluid at the sides [33]. (c) Numerical predictions of the acoustophoretic particle trajectories for particles of (i) 0.5, (ii) 1.2, (iii) 5.2, and (iv) 7.8 μm [34], (d) Particle locations within a 40 μm high chamber. Top: initial positions of particles, middle: position of particles of size 1 μm after 5 s, and bottom: position of particles of size 2 μm after 5 s [35]. Reproduced with permission.

Recently, Das et al. [23] theoretically calculated acoustic body force for a vibrating boundary scenario, showing that it strongly depends upon fluid rheology. Fig. 3a shows the calculated x and y-components of acoustic force density for *De* = 0, 0.2 and 0.4 where Deborah number (*De*) is a measure of extra stress components. Their study found that extra stresses present in the fluid cause a decrease in acoustic force density. This can be used to regulate acoustic body force required for removal of nonspecifically– bound proteins in a compact biosensor platform. Karlsen et al. [33] theoretically predicted the acoustic body force in an inhomogeneous fluid and concluded that it depends on fluid compressibility and gradient of density (Fig. 3b). Their predictions were supported by the experimental results obtained via confocal imaging of the fluid in a microchip. Fig. 3c shows numerical predictions of particle trajectory in a standing SAW-driven PDMS microchannel where 6.67 MHz SAWs were applied via a 128° Y-cut X-propagating $LiNbO_3$ substrate [34]. The microchannel width was 600 μm and height was 125 μm. The numerically-predicted trajectories are in good agreement with experimental results. Devendran et al. [35] numerically computed the trajectories of particles in a PDMS microchannel of height 40 μm and width 400 μm (Fig 3d). They observed alignments of particles along the pressure nodes and, in addition, predicted circulating particle trajectories near the side walls that were in excellent agreement with experimental measurements.

2.4. Bjerknes force

The acoustic radiation force acting on a gas bubble present inside a fluid is called Bjerknes force, named after V.F.K. Bjerknes, who described it for the first time [36]. The Bjerknes force can be classified into two manifestations: (i) the primary Bjerknes force which is experienced by a single bubble in an acoustic field, and (ii) a secondary Bjerknes force which arises due to bubble-bubble interactions. The primary Bjerknes force ($\mathbf{F}_{pB}$) can be expressed as

$$\mathbf{F}_{pB} = -\nabla p_1 V_b \tag{19}$$

where V_b is the bubble volume. Considering oscillations in pressure fields, this primary Bjerknes is usually expressed in time-averaged form as

$$\langle \mathbf{F}_{pB} \rangle = -\frac{4\pi}{3} \langle R^3(t) \nabla p_1 \rangle \tag{20}$$

where $R(t)$ is the bubble radius. Note that bubble radius fluctuates sinusoidally and can be expressed as $R = \bar{R} + \xi \sin(\omega t)$ where $\bar{R}$ is mean radius and ξ is the amplitude of pulsation.

The secondary Bjerknes force ($\mathbf{F}_{sB}$) acts between bubbles and in 1974, L. A. Crum [37] provided an analytical expression for secondary Bjerknes force acting between two bubbles in a stationary wave as

$$\mathbf{F}_{sB} = -2\pi\rho_{f0}\omega^2 \xi_1 \bar{R}_1 \xi_2 \bar{R}_2 \cos(\varphi) \mathbf{r}/d_{12}^3 \tag{21}$$

where subscripts 1 and 2 denote bubbles 1 and 2 respectively; the phase angle between R_1 and R_2 is φ; $\mathbf{r}$ is the vector along the minimum distance between bubbles, and $d_{12} = |\mathbf{r}|$ is the distance between the two bubbles. The negative sign indicates that the secondary Bjerknes force is attractive in nature.

2.5. Acoustothermal heating

Propagation of acoustic waves inside a fluid causes thermal heating as demonstrated by several experimental studies [38–41]. This temperature rise from acoustothermal heating can be theoretically understood

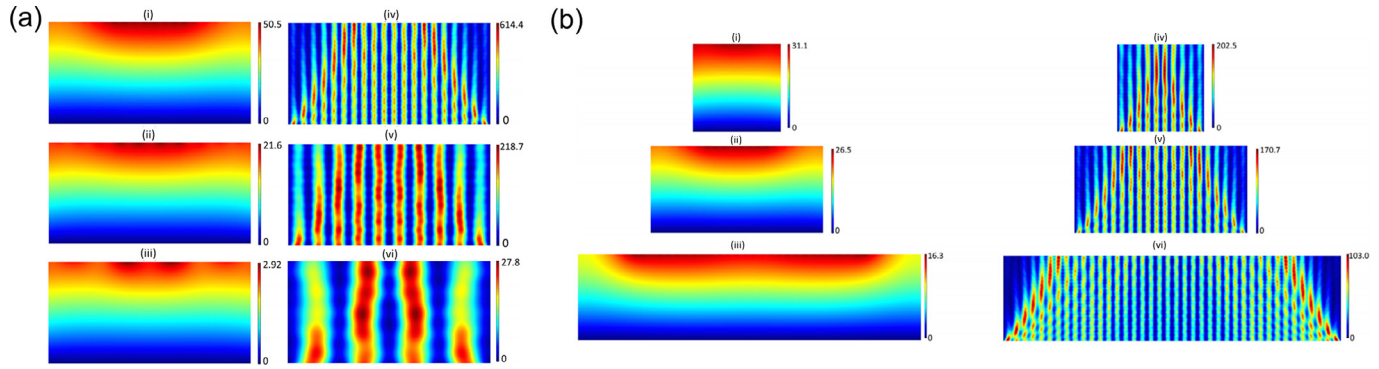

Fig. 4. Second-order temperature in K [(i)–(iii)] and acoustic energy density fields in J/m^3 [(iv)-(vi)] for a standing SAW-actuated closed microchannel of (a) W = 200 μm and H = 100 μm, with SAW wavelength λ = 20 μm [(i) and (iv)], 40 μm [(ii) and (v)], and 100 μm [(iii) and (vi)] for SAW amplitude d_0 = 0.5 nm; (b) aspect ratio δ = 1 (i,iv), δ = 2 (ii,v), δ = 4 (iii,vi); with SAW wavelength λ = 40 μm and SAW amplitude d_0 = 0.5 nm [25]. Reproduced with permission.

from the solution of the second-order equations. In fact, the time-averaged second order temperature T_2 indicates that the acoustothermal temperature rise and the acoustothermal heat flux can be expressed from Eq. (15) as

$$\dot{Q} = \nabla.\left[\langle \mathbf{v}_1.\sigma_1 \rangle - \left(1-\alpha_{p0}T_0\right)\langle p_1\mathbf{v}_1 \rangle + \langle k_1\nabla T_1 \rangle - \rho_{f0}c_{p0}\langle T_1\mathbf{v}_1 \rangle\right] \quad (22)$$

Das et al. [25] theoretically explained the acoustothermal heat generation for the first time. They have studied the acoustothermal temperature rise in a standing SAW-driven PDMS microchannel (Fig 4). Their study showed that acoustothermal heating primarily occurs due to conversion of acoustic energy into internal energy due to pressure work on the fluid and the hydrodynamic transportation of the heat. Viscous dissipation and diffusive thermal transport made insignificant contributions towards the acoustothermal temperature rise.

3. Acoustic wave modes

It was in 1885 that Lord Rayleigh discovered a mode of acoustic wave propagation in which acoustic energy is confined near the surface of an isotropic solid [42]. As a result, such waves came to be known as Rayleigh waves. Besides the shear vertical Rayleigh waves, other types of SAWs that have been used in sensing applications can be generated by IDTs on the surface of a piezoelectric substrate.. These are shear horizontal surface acoustic waves (SH-SAW), flexural plate waves (FPW), Lamb waves, Love waves, and surface-skimming bulk waves (SSBW). A quick overview of the different types of SAWs and their characteristics is given in the following sections.

3.1. Rayleigh waves

Rayleigh waves were initially discovered by Lord Rayleigh by analyzing seismic waves, the waves that move along the surface of the bulk with each particle performing clockwise and counterclockwise elliptical rotations at different depths within a wavelength perpendicular to the bulk surface, to propagate the waves on the surface [42,43]. The amplitude of Rayleigh waves decreases exponentially with depth into the bulk, so that the wave power is largest at the surface [44]. The acoustic energy is confined near the surface, which makes such devices highly-sensitive to surface perturbations and changes, allowing for the measurement of parameters such as temperature, humidity, pressure, viscosity, and mass [45]. The first SAW device was made by R. M. White and F. W. Voltmer in 1965 [6]. They configured interdigital transducer (IDT) patterns on the top of a piezoelectric material to actuate and detect SAWs generated by the piezoelectric effect [6]. Some common applications of SAW devices include communications and electronics for RF filters due their high relative bandwidths and low insertion losses [46]. For biosensing applications, Rayleigh wave devices are preferentially used on gas-phase samples rather than liquid-phase ones due to coupling of the longitudinal component of the Rayleigh waves with the liquid sample, resulting in signal attenuation [47] (Fig. 5a).

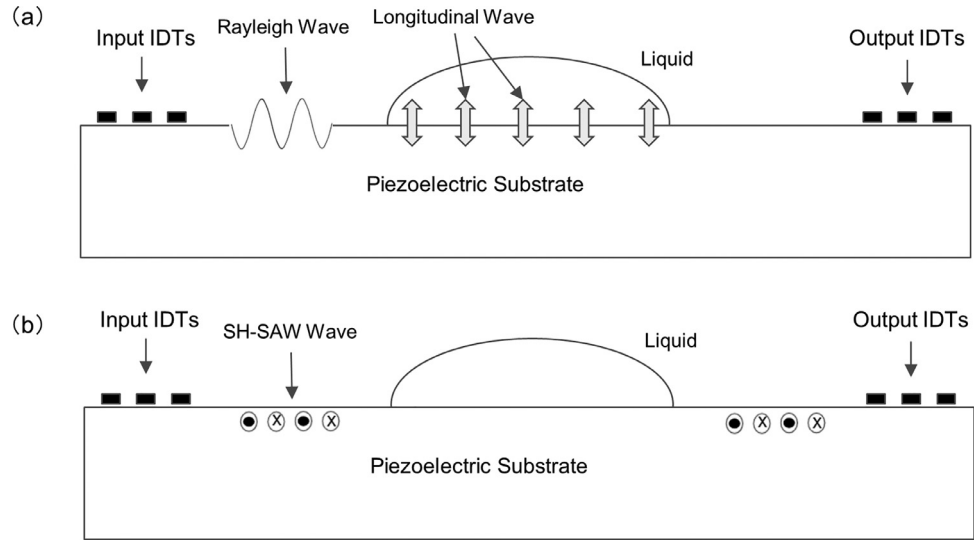

Fig. 5. Schematic diagram showing (a) Rayleigh wave and (b) SH-SAW wave propagations. The particle movement in and out of the plane of the figure is indicated by "cross" and "dot" signs.

3.2. Shear horizontal surface acoustic waves

In 1968, Bleustein discovered shear horizontal surface acoustic waves (SH-SAW) in a hexagonal 6mm class piezoelectric material, barium titanate (BaTiO3) [48–50]. Shimizu then demonstrated a small resonator that adopted SH-SAWs at the edges of a substrate [51]. SH-SAW propagates due to the vertical movement of surface particles relative to the wave propagation direction and surface normal. In terms of sensing capabilities, SH-SAW sensors are generally used for the detection of liquid samples, due to less energy dissipates into the liquid during wave propagation [52] (Fig. 5b). There are many available materials for SH-SAW sensor substrates, such as common piezoelectric substrates like quartz, lithium tantalate ($LiTaO_3$) and lithium niobate ($LiNbO_3$), as well as other crystals such as langasite, $LiBF_4$ and $KTiOPO_4$ (KTP) [53]. When guided with a waveguide layer, SH-SAWs can be converted to Love waves, which is a common approach to reduce energy loss into the substrate and provide high sensitivity to surface disturbance [54,55] .

3.3. Flexural plate waves

To an outside observer, flexural plate wave devices (FPW) are similar in appearance to SAW devices. FPW sensors can be operated at lower frequencies (≈5 MHz) than SAW sensors and they can be used in both liquid- and gas-phase sensing [56]. In addition, the transducers can be placed on the surface opposite the sensing area which allows for the complete isolation of the electronics from the sample [8]. For this to happen, the membrane thickness must be comparable to or smaller than a SAW wavelength to ensure that waves propagate across both membrane surfaces [57]. Measurements in both gas and liquid phases are possible because the FPW velocity is lower than the compressional velocity of sound in liquids. As a result, compressional waves are not coupled to the adjacent liquid and only minor energy dissipation occurs. FPW sensors are highly mass-sensitive, but for practical, high-sensitivity mass measurements, the membranes have to be very thin (on the order of a few micrometers which renders them fragile and difficult to handle and fabricate [58]. For this reason, they are not popular in acoustic wave sensing applications.

3.4. Lamb waves

Lamb wave sensors generally have a high sensitivity to surface changes. Lamb waves are plate-guided and can be seen as a combination of two propagation waves that are separated by the guiding plate [43,59,60]. Lamb waves occurs when the plate thickness is greater than two acoustic wavelengths, and all Lamb wave modes can be categorized as either symmetric (or S0) or asymmetric (A0) [1,61]. In A0 mode, which is usually operated at low frequencies (5–30 MHz) where phase velocity is lower than the longitudinal wave velocity in liquid media, the acoustic energy is not coupled to the liquid [1,59,61]. When the thickness of piezoelectric substrate is low, A0-mode acoustic energy converges on the surface of the sensor, making it highly sensitive to surface perturbations [45]. Because of this, Lamb wave sensors can be useful in liquid sensing.

3.5. Leaky-SAWs

Leaky-SAWs (LSAWs) can also be generated by IDTs at the surfaces of some piezoelectric materials and are usually indistinguishable from

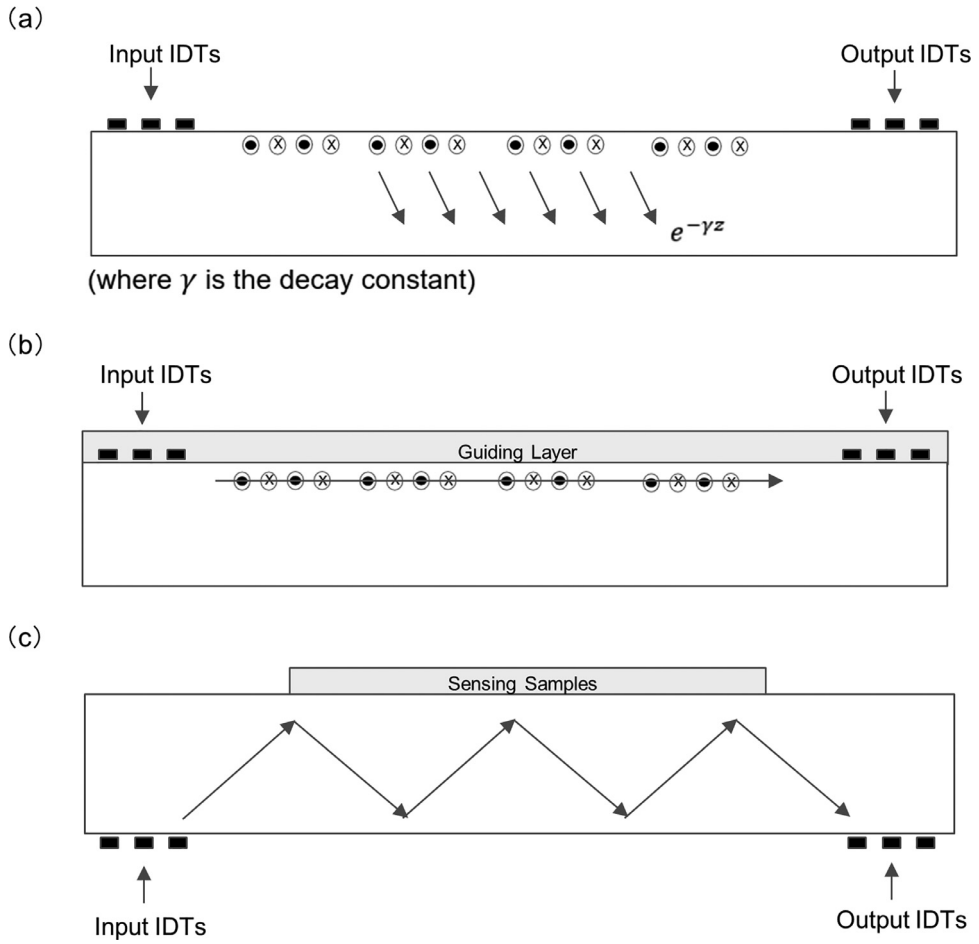

Fig. 6. Artistic representation of some SAW types: (a) SSBW; (b) Love wave; (c) SH-APM. For polarization direction along the *x*-axis, the particle movement in and out of the plane of the figure is indicated by "cross" and "dot" signs, respectively [1,71].

Rayleigh waves. As this mode propagates along the surface of the substrate, a fraction of the wave's energy travels within the substrate depth and therefore is attenuated in the propagation direction. The resulting energy leakage from the surface is the reason for this mode's name. LSAW modes with shear horizontal displacement have been identified for specific rotations of $LiTaO_3$ and $LiNbO_3$ [62,63]. It has been shown that LSAWs can be used for liquid-based sensing due to the predominantly shear horizontal particle displacement [64] and thus energy losses due to the radiation of compressional waves into the liquid can be avoided. However, a thin metal film must be coated on the propagation path to counteract losses that occur due to the energy leakage into the bulk crystal [65].

3.6. Surface skimming bulk waves

In addition to surface waves, IDTs also generate a significant amount of bulk wave radiation. Bulk wave radiation in SAW devices produces unwanted signals that transfer energy to the output transducer at different frequencies and different delays from those of the SAW signal [66]. Surface skimming bulk waves (SSBWs) are acoustic waves with shear-horizontal particle displacements that travel just below the surface of the substrate (Fig. 6a). Because of their propagation into the bulk of the piezoelectric material, SSBWs suffer considerable acoustic loss [67]. The wave is also less sensitive to surface perturbations [68], and high noise levels are present at the output due to diffraction of the signal into the bulk substrate and reflections off the lower surface of the crystal [69]. There are two ways to combat these problems. One is to place a corrugated surface in the delay path between the IDTs, to slow down the SSBW and convert it into a surface wave [70]. A second method involves the application of a thin dielectric material overlaying the surface for the same purpose. SSBW devices have a couple of advantages over conventional SAW devices. First SSBWs have higher velocities which allows devices to operate at fundamental frequencies of up to about 60% higher than a conventional SAW device with identical IDT geometry [68]. Secondly, SSBWs have superior temperature coefficients for certain crystal cuts of quartz and $LiTaO_3$ [71]. Examples of SSBW devices used for biosensing applications can be found in references [69,72,73].

3.7. Love waves

Another type of type of horizontally polarized shear SAW is the Love wave named after Augustus Love who predicted their existence in 1911 [74]. For a Love wave to exist there must be a finite thick layer over a semi-infinite substrate and the shear horizontal bulk wave velocity in the layer must be less than that in the substrate material [75]. When this happens, the layer slows down the acoustic shear mode in the substrate so that the penetration depth is decreased and the acoustic energy is confined to the surface [76] (Fig. 6b). Mass sensitivities of Love wave devices depend on the operating frequency, waveguide material, and the thickness of the waveguide normalized to the wavelength [77,78].

Examples of polymer materials used as guiding layers are PMMA [79,80], polyimide [81], and photoresists [82,83]. Polymers have an advantage over other waveguide materials because of their low shear wave velocities compared to typical piezoelectric substrates [69] and the ease of surface layer preparation [84]. However, a disadvantage is that they are usually lossy [85]; acoustic absorption increases quickly with increasing layer thickness that can eventually result in an insertion loss that is greater than in uncoated devices [69]. Piezoelectric thin films like ZnO have also found use as guiding layers [86–88]. Because it is a piezoelectric material with a low phase velocity (2650 m/s), ZnO can increase the electromechanical coupling coefficient more than other deposited materials [86].

Photoresists have also been utilized as waveguide layers. As additional protection against harsh liquid environments, one research group deposited a layer of SU8 photoresist over the sensor surface [89]. The waveguide can also act as a shielding layer to protect the electrodes from the liquid environment-particularly when aluminum is used [81]. When detecting in liquid, there are a number of interactions that can perturb the propagating acoustic wave: mass, viscosity, and the electric and dielectric properties of the interface. Therefore, a three layer system that incorporates a thin gold layer on top of the waveguide can be used to eliminate the acoustoelectric interaction and more closely represent a pure liquid mass sensor [19].

3.8. Shear horizontal acoustic plate mode waves

Shear Horizontal Acoustic Plate Mode (SH-APM) sensors are common bulk acoustic wave devices. Rayleigh and shear horizontal waves can both be actuated at different frequencies and their superposition will reflect at a certain angle at the upper and lower surfaces, causing the propagation of APM waves within the bulk [90–92] . APMs are composed of several plate modes with different frequencies, andhe frequencies of the SH-APM mode are inversely related to the plate thickness. For this reason, plate thickness is usually within several wavelengths of the operating frequencies. Increasing plate thickness beyond this point would decrease the gaps between different mode frequencies to the point where only Rayleigh waves would be distinguishable [90]. SH-APM can be useful in liquid-based detection since there is no vertical displacement component during the wave propagation [91]. One advantage of SH-APM is that both upper and lower surfaces can be used for sensing, so that liquid sample can be loaded on the opposite side from the IDTs so that corrosion of electrodes is minimized (Fig. 6c) [93].

4. Advanced functional devices

The conventional SAW devices typically consist of dual delay line configurations with one delay line used as a reference to compensate for environmental variations [1,7,94]. Experimental and theoretical efforts have focused on the design and fabrication of acoustic wave devices which can allow for better sensor characteristics as well as materials characterization possibilities [79,95,96]. Integrated multidirectional inter-digital transducers (IDTs) and delay path modifications for SAW sensors in a piezoelectric substrate have been developed and have been shown to positively and significantly impact power consumption, device sensitivity, and bio-fouling elimination capability. Here, we review some of the advanced sensor designs that have been aimed at eliminating biofouling phenomena and improving biosensor performance.

This section reviews advances in transducer and electrode designs that have led to the development of multidirectional transducer-based SAW devices on a single piezoelectric substrate which potentially offer the advantage of selectively exploiting features specific to acoustic waves propagating along a given crystallographic orientation.

4.1. Hexagonal surface acoustic wave device

Cular et al. have developed a sensor device with a complicated transducer design in the hexagonal SAW sensor as shown in Fig. 7 [97]. This device is comprised of three different delay paths (each has a pass band frequency at 97 MHz) which are aligned in a manner such that it allows for generation of acoustic waves which are different in character [98]. It is possible to exploit the anisotropy of the piezoelectric substrate to generate multiple wave modes and develop SAW devices that can serve as better chemical and biosensor elements.

There are several advantages to the fabricated hexagonal SAW device. The three different delay paths could be used for simultaneous detection and the data collected across the three delay paths allows for better characterization of the sensing (thin film) material. This design allows for the simultaneous extraction of multiple properties (e.g. film material density or thickness, Lamé and shear moduli, and sheet conductivity) of a thin film material to achieve a more complete characterization than when a single SAW device is utilized [97]. Thus, these devices can serve as better in-situ characterization tools in thin film physical and chemical deposition equipment. In sensor applications, this capability

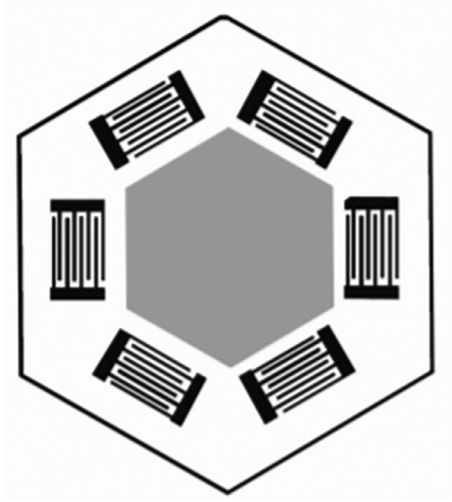

Fig. 7. Hexagonal SAW device used for chemical and bio-sensing applications as well as in materials characterization.

was shown to translate into better discrimination of the analyte and more accurate determination of the concentration. Experimental results by Cular et al. have shown increased sensitivity for these devices when used as a chemical sensor to detect the concentrations of hexane, chloroform and benzene [97]. Other application of the hexagonal SAW in biosensing involves the ease of detection as well as removal of non-specifically bound proteins (acoustic streaming) enabling the repeated use of sensor device [138], and in more accurate determinations of analyte concentrations. In such a device operation, one of the delay paths makes use of shear horizontal SAW waves for detection whereas the other delay paths with a dominant Rayleigh mode are used to simultaneously remove the nonspecifically-bound proteins using acoustic streaming. The fabrication of a hexagonal SAW device can be carried out on any piezoelectric substrate such as lithium tantalate and lithium niobate. The choice of a delay path for any specific application depends on the propagation characteristics of the wave generated along the crystal cut and orientation corresponding to that delay path. In principle, with identified crystallographic directions on a given piezoelectric substrate, it would enable fabrication of a hexagonal SAW device that can be functional in both gas and liquid phases, and the same device could be used for chemical and biosensing applications.

4.2. *Orthogonal surface acoustic wave device*

Computational modeling by Singh et al. on an orthogonal SAW device based on LGS indicated that differing characteristics of acoustic waves (Fig. 8a) propagating in different Euler directions could facilitate target analyte detection and simultaneous NSB protein removal in the same sensing area [99]. In the simulated device, they showed that the (0, 22, 90) direction is suitable for biosensing and the (0, 22, 0) direction for potential application in NSB protein removal via acoustic streaming.

Singh et al. performed detailed theoretical analyses of the wave propagation characteristics in orthogonal SAW design based on LGS substrates [99]. Propagation along the (0, 22, 90) direction indicated shallow penetration depth, rendering the biosensor suitable for liquid sensing applications. (Fig. 8b). On the other hand, the (0, 22, 0) direction showed the presence of mixed modes (Fig. 8c). Despite the wave mode being mixed, the surface normal component was found to be in the (0, 22, 0) direction. This suggests strong coupling with the fluid domain and can be utilized to remove NSB proteins from the device surface using acoustic streaming [99].

The finite element model developed by Singh et al. was also utilized to calculate the device sensitivity for various piezoelectric devices [100]. It was found that the computed sensitivity along (0, 22, 90) direction to a 100 pg applied mass was higher for the LGS device in comparison to a SAW device based on the competitive and practical 36° YX $LiTaO_3$ [101] substrate (11.09 Hz-cm^2/ng vs. 2.98 Hz-cm^2/ng, details shown in Fig. 9).

Orthogonal IDT designs have been utilized in several applications in recent years. Liu et al designed a novel MEMS-IDT gyroscope with SAW resonator IDTs and SAW sensor IDTs in an orthogonally-patterned device [103]. The SAW gyroscope operates at 96.9 MHz and can detect two orthogonal angular velocities [103]. Ding et al patterned two orthogonal pairs of IDT resonators on a $LiNbO_3$ substrate to manipulate polystyrene particles and a 6 μm single bovine red blood cell [104]. Similarly, Lee et al implemented a logic switch by using graphene as channel material to manipulate the flow direction of acoustoelectric current [105]. In biosensing applications, Li and Bhethanabotla have recently developed an orthogonal SAW sensor fabricated in ST quartz to achieve protein detection and NSB protein removal from the same sensing area [10]. This orthogonal SAW device can simultaneously actuate Rayleigh waves and SSBWs in orthogonal directions. NSB proteins can be removed by acoustic streaming using the Rayleigh waves, and the SSBWs are brought up to the sensor surface by coating a 100 nm gold film waveguide layer in order to quantify dissolved biomarkers (mouse anti-rabbit IgG) from phase shift measurements. The operating frequency for the sensing channel of this device is 118.22 MHz and that of the removal channel was measured to be 77.66 MHz. Portable electronics were designed and fabricated to accommodate the orthogonal SAW sensor by integrating multiple functions such as signal synthesis, gain control, phase/amplitude measurement, and data processing. This orthogonal SAW detection system has the potential for monitoring biomolecule behavior and quantifying biomarkers in point of care devices [10].

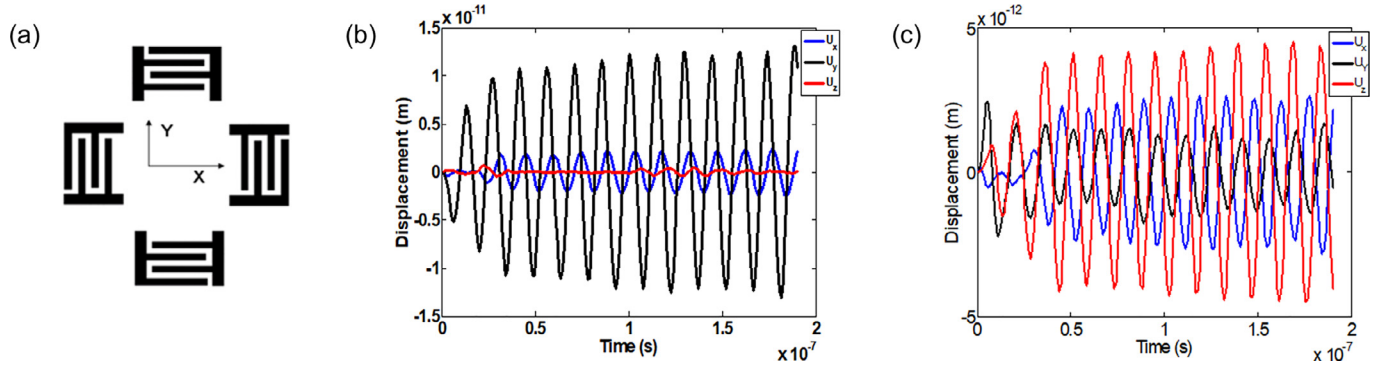

Fig. 8. (a) Schematic diagram of an orthogonal surface acoustic wave device simulated by Singh et al. [99] X and Y denote (0, 22, 90) and (0, 22, 0) directions in the langasite substrate, respectively. Each of the delay paths were simulated independently and the device has a central frequency of 68 MHz; (b) Displacements along the (0, 22, 90) direction; and (c) Displacements along the (0, 22, 0) direction. Reproduced with permission.

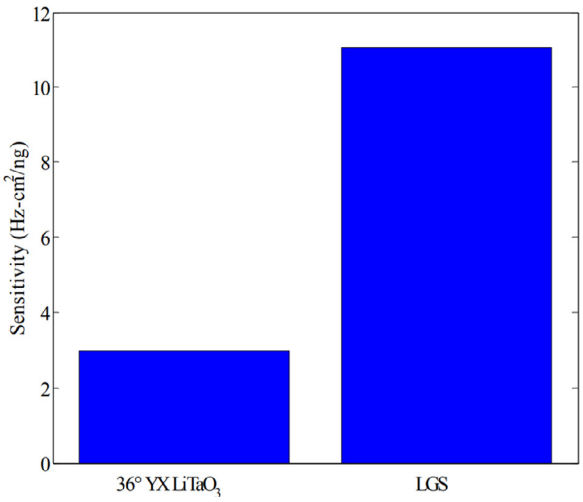

Fig. 9. Comparison of sensitivities for the langasite substrate for propagation along the (0, 22, 90) Euler direction and a comparable 36° YX-$LiTaO_3$ substrate [102]. FE models were created for 100 pg mass applied over an area of 9600 μm^2 in the delay path of the SAW device based on langasite. Transient analysis was used to study transmission characteristics of this ideal mass perturbation sensor. The sensitivity obtained for the LGS SAW device in this study is comparable to that of the 36° YX $LiTaO_3$ device obtained by Cular et al. [101], using the same approach. The sensitivity for the 100 MHz 36° YX $LiTaO_3$ device is scaled to match the center frequency (68 MHz) of LGS. Reproduced with permission.

4.3. Focused surface acoustic wave devices

Studies have indicated that SAW devices with focused interdigital transducers can be used to excite waves with high intensity, high beam-width compression ratio, and small localized area [106–109]. These high-amplitude waves can be utilized to increase the induced streaming velocities to facilitate fluid-based micro-mixing and acoustic radiation force-induced micro-transport for particle sorting and separation. Similarly, acoustically-focused two-dimensional micro-machined micro-droplet ejector arrays fabricated on piezoelectric substrates were able to achieve formation of focal points by leaky SAWs [110]. This allowed for the controlled generation and ejection of picolitre droplets for spinless photoresist deposition.

Altering the transducer electrode design from linear to circular focuses the acoustic energy of the SAW device [102] (Fig 10a). This results in higher-amplitude waves; correspondingly, larger streaming velocities can be generated. Such an electrode configuration could be utilized in multidirectional transducer-based devices to enhance streaming conditions along one of the delay paths. Singh *et al.* have developed 3D computational models to evaluate the enhancement in streaming on the surface of a 100 MHz focused SAW device (F-SAW) and evaluated their utility towards nonspecific protein removal [102]. Their study suggests significant enhancement in acoustic streaming in their F-SAW device when compared to conventional ones; the increase in streaming velocities was computed to be 352% and 216% for tangential velocities in the propagation and transverse directions, respectively, and 353% for the normal velocity. The induced streaming force for F-SAW is 480% higher than for conventional SAW [102]. In biosensing applications, this allows for the removal of smaller sub-micron sized particles by F-SAW which are otherwise difficult to remove using the conventional SAW; the F-SAW presents an order of magnitude reduction in the smallest removable particle size compared to the conventional device. Collins et al. used a focused SAW device on a lithium niobate substrate to create a region of 25 μm to sort particles of a 2 μm size by operating at a frequency of 386 MHz (Fig 10b). The focused IDT has been able to create a displacement region in the center of the fluid channel that is used for particle sorting (Fig. 10c) [111]. Their study indicated that the acoustic energy focusing and acoustic streaming enhancement brought about by the F-SAW device manifests as enhanced streaming efficiency of F-SAWs throughout the device delay path compared to conventional SAWs which enhances sensitivity, selectivity, and reusability.

4.4. Delay path modifications

One of the ways of improving sensor device performance is to introduce delay path modifications and positively alter the propagation characteristics of the acoustic wave. Common methods of decreasing insertion loss and improving wave propagation efficiency in SAW devices include utilization of reflective gratings [112], grooves and corrugated gratings [68,113,114], and wave-guides [115]. The recurring concepts in these four primary methods to reduce power losses are the conversion of bulk waves into surface waves, and entrapment of energy near the surface that would otherwise be lost to bulk waves [112,116].

Integrated multi-directional inter-digital transducers (IDTs) and delay path modifications for SAW sensors in a langasite substrate have been shown by Singh et al. to significantly impact power consumption,

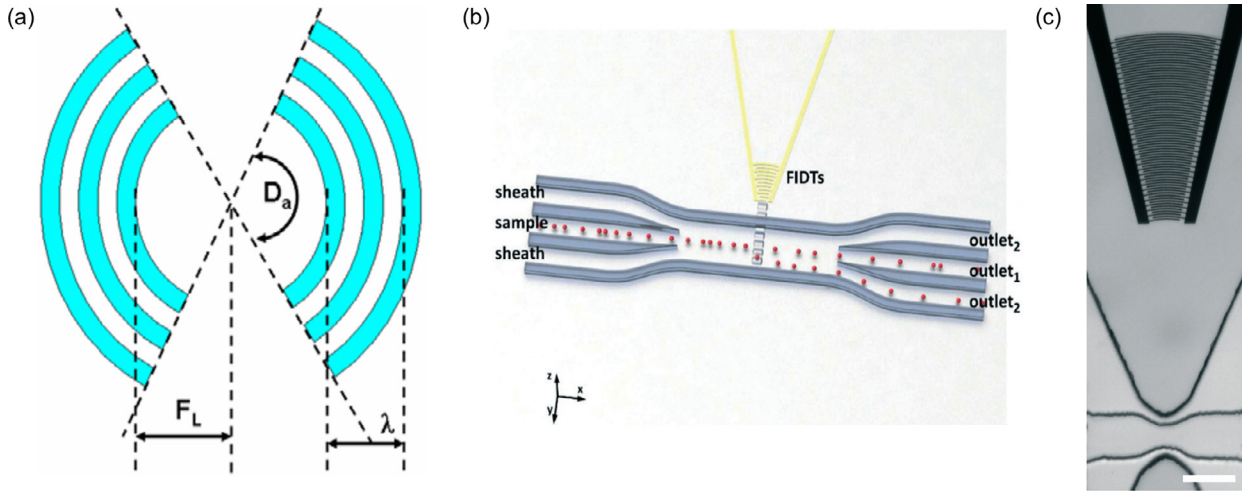

Fig. 10. (a) Schematic illustration of focused IDTs, arc angle, focal length and wavelength are denoted as D_a, F_L, and λ, [102] (b) A focused IDT structure is able to generate a displacement region at the center of the fluid channel [111], (c) A schematic illustration of sorting process – the particles were initially aligned at the center of channel before F-SAW was used to differentiate and displace particles of different sizes [111]. Reproduced with permission.

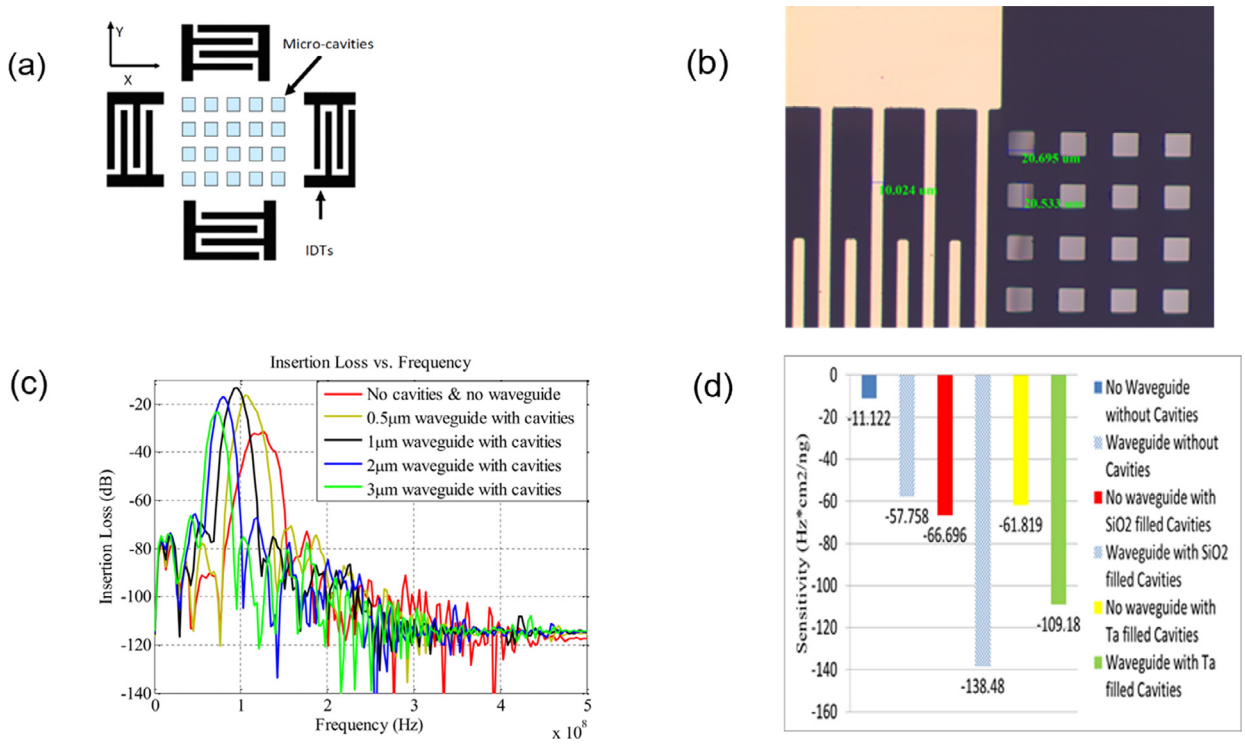

Fig. 11. (a) Schematic diagram of a mutually interacting orthogonal IDT device with microcavities etched along the delay path of the SAW device [102]. The device is not drawn to scale. X- and Y- directions denote different crystallographic directions allowing for propagation of waves of different characteristics. (b) Dimensions of IDTs and tantalum-filled microcavities in the delay region for a fabricated ST quartz SAW chip [16], (c) Improved insertion losses with waveguides and different depths of tantalum-filled microcavities [16], (d) Sensitivity improvements with waveguides and microcavities. Reproduced with permission.

device sensitivity, and bio-fouling elimination capability (Fig. 11a) [102]. In their calculations, the simulated devices were comprised of mutually interacting orthogonal IDTs and micro-cavities of square cross-sections of size $\lambda/2$ at different depths located in the middle of the delay path. A combined orthogonal IDT/polystyrene-filled microcavity device (of dimensions $\lambda/2 \times \lambda/2 \times \lambda/2$), with constructive wave interference and enhanced surface acoustic wave entrapment in the delay region, was shown to be most efficient. This advanced sensor configuration showed a reduction in insertion loss by 23.6 dB, generated two orders of magnitude larger streaming forces, and exhibited velocity sensitivities 100% larger than those of a simulated standard SAW sensor with unidirectional IDTs along the (0, 22, 90) direction [102]. Experimentally, Li et al., using tantalum and silica for filling a microcavity array in the delay path of a ST quartz SAW device, observed a 5 dB reduction in insertion loss and a 10-fold improvement in sensitivity compared to SAW devices without microcavity modification [16] (Fig. 11b–d).

As mentioned in a previous section, SH wave modes can be converted into Love waves through the application of a thin acoustic guiding layer or waveguide [116]. To support this type of wave, the guiding layer must have a shear velocity less than that of the substrate [76]. As the thickness of the guiding layer is increased, the acoustic wave is expected to shift from its propagation within the substrate to propagating within a confined depth at the substrate surface or within the guiding layer. When this occurs, the velocity decreases, causing a negative shift in the fundamental frequency accompanied by an additional decrease due to mass loading of the waveguide [82]. In addition to a lower shear velocity, an ideal waveguide material should have the following properties: (1) low density; (2) low acoustic loss at the operating frequency; (3) chemical stability in an aqueous environment; and (4) strong and specific interaction with an analyte of interest [117]. Dielectric materials such as silicon dioxide (SiO_2) [76,85], silicon nitride (Si_3N_4), and most polymers can be used as waveguide materials.

4.5. *Flexible surface acoustic wave devices*

Recently, flexible SAW devices have drawn attention from researchers due to their potential applications in wearable, recyclable, and disposable electronics. Several groups have fabricated flexible SAW devices by depositing ZnO and AlN films on various polymers such as polyethylene terephthalate (PET) [118,119], polyethersulfone (PES) [120], polytetrafluoroethylene (PTFE), polyimide (PI) [121], and polyethylene naphthalate (PEN) [122]. A fundamental challenge involved in developing flexible SAW devices is the growth of high-quality c-axis-oriented ZnO and AlN films on these polymeric substrates. Propagation of acoustic waves in flexible SAW devices also significantly depends on the polymer substrates. Akiyama et al. [123] demonstrated the effect of pressure variation on piezoelectric effect in a polyimide-based AlN thin-film SAW device. Lamanna et al. [60] fabricated AlN thin films on thermoplastic PEN substrate by low temperature sputtering and observed two resonant modes (Rayleigh and Lamb waves) (Fig. 12a and b). These authors have demonstrated their device in temperature sensing for the temperature range of 25-100°C. In a later study, Lamanna et al. [124] also presented their AlN/PEN-based flexible SAW device as a biosensor for the detection of E-coli at 500 MHz Lamb wave frequency and compared the results to those from an AlN/silicon device (Fig. 12c and d). This inexpensive device fabricated on a flexible substrate could be useful in food packaging applications. These authors achieved an LoD of 6.54×10^5 CFU/ml for their flexible SAW device whereas the LoD for AlN/silicon device was found to be 1.04×10^6 CFU/ml. Zhou et al. [125] fabricated ZnO-based SAW devices on a polyimide substrate and reported the effects of deposition conditions and ZnO film thickness on its performance. Despite this progress, fabrication of flexible SAW device is still a challenging task and requires significant effort due to the large mismatch in thermal expansion coefficients between piezoelectric material and polymer substrates, poor adhesion of piezoelectric films on

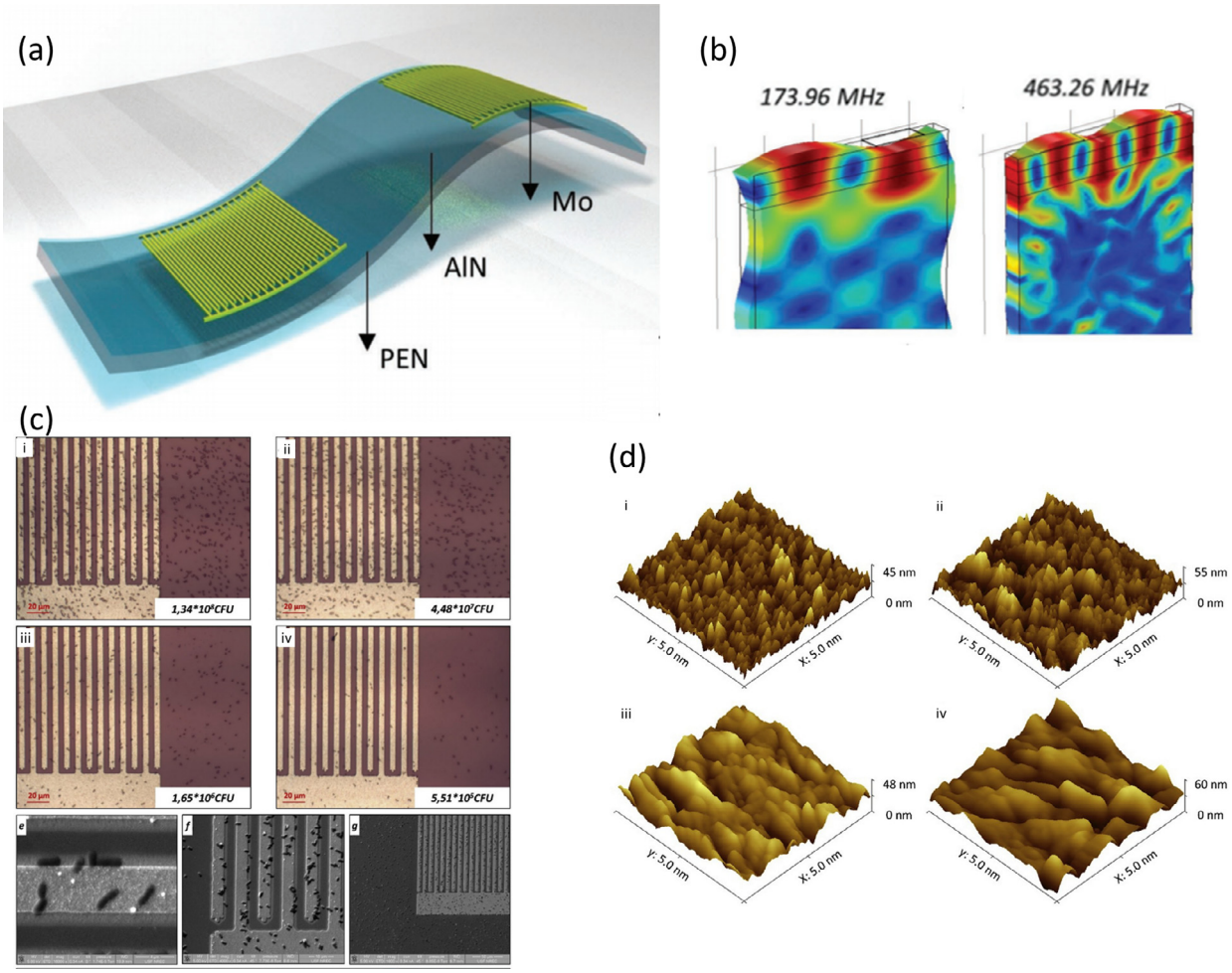

Fig. 12. (a) A schematic of an AlN-based flexible SAW device; (b) FEM simulation of Rayleigh and Lamb wave propagations at 173.96 and 463.26 MHz, respectively [60]; (c) An optical micrograph of the bacteria adhesion at increasing concentration (i-iv) and SEM imaging of the grafted bacteria at 16k, 4k, and 1k magnifications, respectively (e-g); (d) AFM images of AlN surface on silicon and PEN, respectively (i-ii), and functionalized AlN surface on silicon and PEN, respectively (iii-iv). [124]. Reproduced with permission.

polymer substrates, and high attenuation/dissipation of acoustic waves into the polymeric substrates.

5. SAW applications in biosensing

5.1. Vapor and small molecule detection

SAWs can be used for vapor and biomolecule detection by observing frequency shifts from very small mass loading of analytes, and the frequency shift can be calibrated with mass loading on SAW surface down to a picogram level [55]. Covalently attaching biomolecules to the surface offers several advantages such as stability and reproducibility of bioreceptors [126]. For example, by coating 3 different odorant binding proteins (OBPs) to an array of 5 SAW resonators, the relative changes in resonant frequency can be used to detect the concentrations of octenol and carvone vapors [127]. SAW sensors functionalized with olfactory receptors to improve sensitivity can also detect diacetyl. With a 10 nm gold coating on $LiNbO_3$-based SAW sensor, ODR-10, an olfactory receptor of *Caenorhabditis elegans*, was coated on the sensor surface to sequester diacetyl. Sensitivity to diacetyl concentration, as measured by the frequency shift of the SAW signal, can be as high as 2 kHz/ng and the detection limit decreased to 10×10^{-10} mM [128]. Hasanuddin et al. has developed a fruit ripeness system using zinc oxide as a sensitive layer [129]. The lithium niobate-based gas sensor can determine different maturity levels of fruits by detecting ethylene [129]. Potential SAW-based gas sensor research directions include improving the stability of substrate, selecting circuit electrode materials that can accommodate harsh sensing environments, and using advanced sensing materials/multiple SAW resonator arrays for complex gas detection and quantification [130].

5.2. Cell lysis with SAW

Some biosensing applications require the disruption of cells so as to release intercellular materials such as DNA, RNA, or proteins for the detection of pathogens and in point of care diagnostics. In biomedical applications, the increased demand for miniaturized systems is often associated with a need for more sophisticated ways to lyse cells in microscale volumes, for which acoustic waves offer a robust approach. Ultrasound is traditionally used for cell lysis but requires bulky high-power equipment and relatively high sample volume (~ml). Several attempts have been made to reduce the sample size and power consumption by using bulk acoustic waves (BAW) [131]. However, surface acoustic waves show even higher efficiency and require even less sample volume than BAWs due to surface trapping of acoustic energy. Taller *et al.* reported the use of SAWs for exosome lysis and RNA detection in a pancreatic cancer study [132] (Fig. 13a). In that work, twenty pairs of titanium/aluminum IDTs were used to generate Rayleigh SAWs in one direction in a 127.68° YX cut lithium niobate ($LiNbO_3$) substrate. The operating frequency was 28.3 MHz and the sample was exposed to the

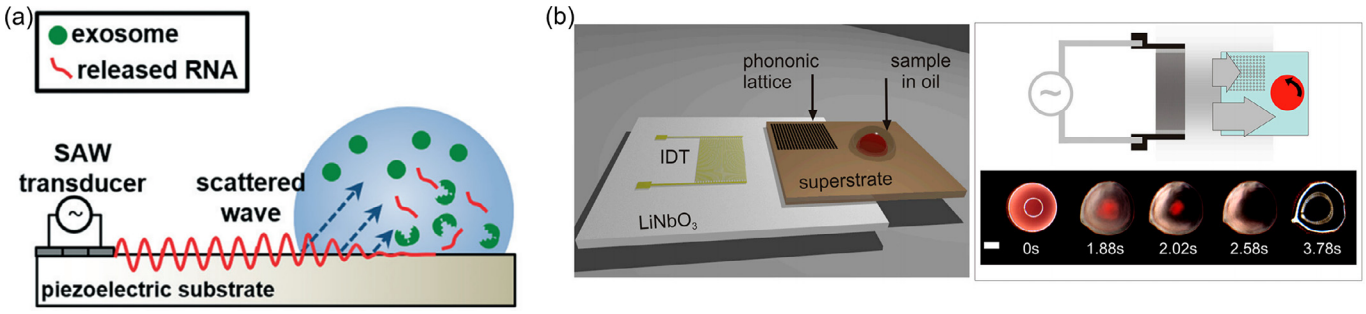

Fig. 13. (a) Schematic of SAW-based lysing of exosomes to release RNA for detection [132]; (b) Integrated set up for cell lysis and PCR testing where a microliter-sized droplet is positioned on a superstrate and coated with a layer of oil to prevent evaporation during processing [133]. Reproduced with permission.

SAW for 30 s at 1 W power which resulted in a 38% lysis rate sufficient to obtain the requisite exosomal RNA. Reboud et al. [133] used SAW generated on a $LiNbO_3$ piezoelectric substrate and coupled that onto a phononic superstrate which acted as a frequency-tunable filter (Fig. 13b). In that study, a 5–20 μl droplet containing blood cells was placed on the superstrate and the SAW was actuated at a 9.5 MHz frequency with a power of 3.1 W. They reported >98% lysis rates for sample volumes ranging from 10 to 20 μl whereas a 5 μl sample showed ca. 50–98% lysis rate depending upon the dilution factor. The study also investigated the lysis of mammalian HL60, MCF7 cells expressing a GFP-actin fusion and a trypanosome (T. cyclops) at 9.61 MHz frequency with SAW power varied between 0.06W to 0.8 W. For these cases, the cell lysis was observed for power > 0.3 W; at 0.8 W *ca.* 98% lysis rate was achieved. However, SAW-based lysis has limitations as it generates heat and significant heating can denature proteins. Hence, proper tuning of device frequency and operating power is required for effective lysis.

5.3. Monitoring of cell adhesion

Cell adhesion provides valuable information regarding cell activity and function and is important for many medical purposes such as bone repair and tissue assembly [134,135]. Characterization of cell adhesion can be performed by measuring the binding affinity of proteins that are present on the surface of a cell [136]. By measuring phase and amplitude variation, SAW-based methods can detect the binding kinetics of coupling and decoupling rates, the equilibrium dissociation rate, and conformational changes due to the binding. Generally, binding-induced mass loading at the surface of SAW sensor will result in a phase change and the change in viscosity from the bound biomolecule to the sensor surface will result in an amplitude change [137]. An application of a Love wave system has also been developed by Saitakis, Dellaporta and Gizeli to monitor the cell adhesion to sensor substrate by observing the frequency change due to energy dissipation [138]. In their experiment, a PMMA polymer guiding layer is first attached on top of the quartz-based Love-wave biosensor. On top of the PMMA guiding layer, a thin gold layer is then deposited to immobilize a biorecognition layer [138] as shown in Fig. 14. Following that, anti-HLA antibody is immobilized

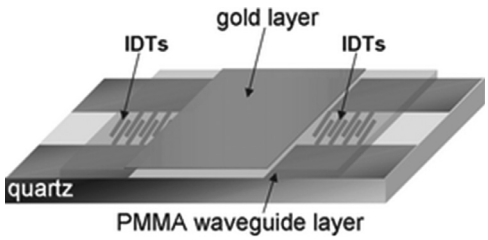

Fig. 14. Schematic of Love-wave biosensor. Two interdigitated transducers (IDTs) are deposited on quartz-based sensor. Polymethylmethacrylate (PMMA) is attached in between IDTs as a wave guiding layer, followed by a thin gold layer [138]. Reproduced with permission.

to Protein G conjugated on the gold surface. The response of analyzed ligand receptor, HLA-42, increases the amplitude (dB) of the Love wave sensor as more HLA molecules bind to the surface. The mass loading process of small molecules to ligands is very sensitive and produces a real-time response [138].

5.4. Separation of cells and particles

Sorting of particles and cells constitute essential steps in many biomedical applications and a significant amount of research effort has been extended over the last century to improve its method and efficiency. Among the available methods, invasive ones such as filtration and pinch flow margination require relatively simpler equipment setup and costs. However, they cannot provide the flexibility required for microscale operations and hence, noninvasive methods involving magnetic, electric, or acoustic fields are extensively used for these applications. The high scalability and cost-effectiveness of acoustic field-based particle separation techniques makes it a more attractive approach for many applications. The most common acoustic wave modes used for particle or cell separation are SAW or shear mode. In SAW-based devices, a standing wave field can be created via two pairs of IDTs which generate two SAWs traveling in opposite direction. This SAW, in contact with the fluids, refracts and creates pressure wave within the fluids where minimum and maximum pressure regions are called pressure nodes and antinodes, respectively. Primary acoustic radiation force, generated due to pressure wave, can attract or repel particles towards pressure nodes and antinodes, based on their density and sizes. For spherical particles, primary acoustic radiation force in a standing wave field is given by Yosioka and Kawasima [31]

$$\mathbf{F}_R = -\frac{2\pi^2 a^3 \kappa_f p_1^{\,2}}{3\lambda}\phi \sin\left(\frac{4\pi \mathbf{x}}{\lambda}\right) \tag{23}$$

where acoustic contrast factor, $\phi = \frac{5\rho_p - 2\rho_{f0}}{2\rho_p + \rho_{f0}} - \frac{\kappa_p}{\kappa_f}$; λ and $\mathbf{x}$ are the SAW wavelength and position of particle from pressure node, respectively. Hence, positive and negative contrast factors direct the particles towards pressure node and antinodes, respectively. Particle size, SAW wavelength and fluid compressibility determine the magnitude of the acoustic radiation force required for controlling the migration time and position of the particles. Nam et al. [139] reported separation of platelets from whole blood using a standing SAW-based microfluidic system with 0.25 μL/min flow rate and achieved 98% purity in platelets (Fig. 15a). Li et al. [140] were successful in separating circulating tumor cells (CTCs) from clinical patient samples using tilted angle SAW technique (taSAW) (Fig. 15b), although the throughput was maintained at 20 μL/min which was relatively low for practical applications. In a later study, Wu et al. [141] isolated CTCs at a higher throughput of 125 μL/min using an optimized standing SAW-based acoustofluidic platform wherein a piece of glass was inserted at the ceiling of the microfluidic channel to form a vertical acoustic resonator (Fig. 15c). Other than platelets and CTCs, SAW devices have also shown potential in separating bacteria from blood or sputum samples and thereby may play a crucial role in

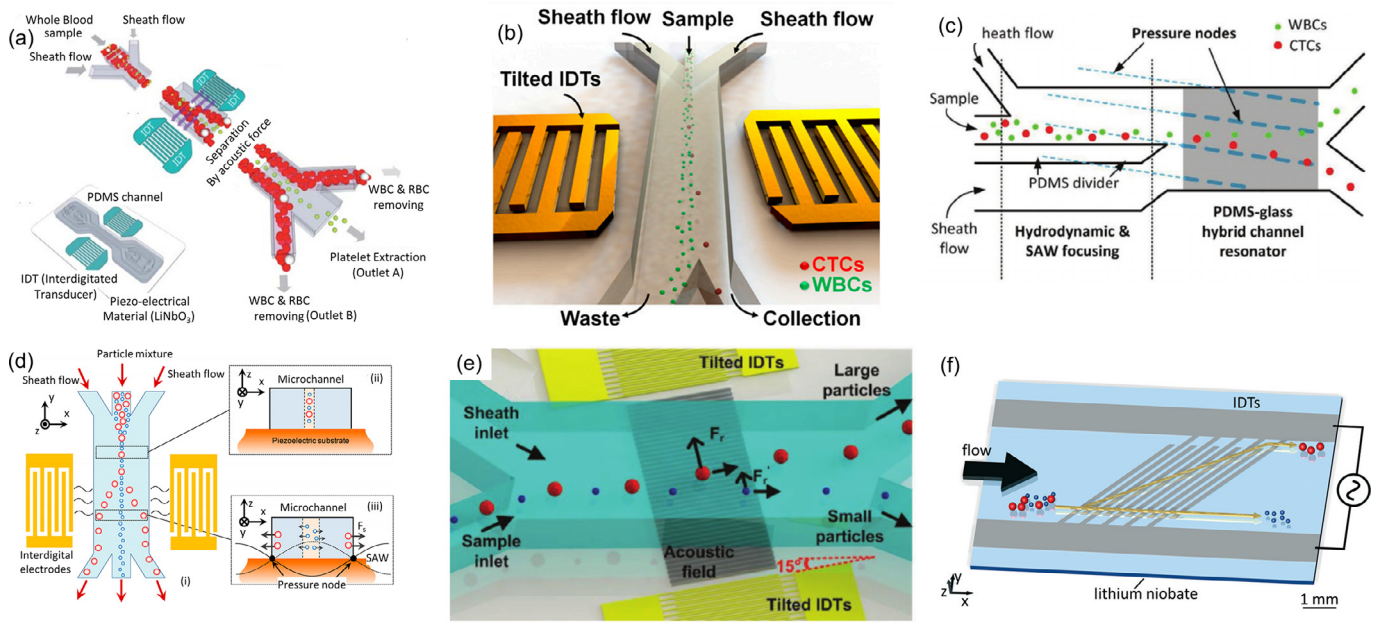

Fig. 15. Schematic illustration of (a) a standing SAW device for platelet separation from whole blood samples [139], (b) a high-throughput taSSAW device for cancer cell separation [140], (c) a SAW based microchannel for CTC separation [141], (d) a microfluidic channel for E. coli separation from blood cells [126], (e) an acoustic-based nanoparticle separation device [143], and (f) a vDLD operation for particle separation [144]. Reproduced with permission.

pathogen identification or sepsis diagnosis. Ai et al. [126] reported separation of *Escherichia coli* from blood cells using a standing SAW device and obtained purity of separated *E. coli* to be 95.65% with a flow rate of 0.5 μL/min (Fig. 15d). Using a similar technique, Li et al. [142] were able to isolate *E. coli* from blood with more than 96% purity. The SAW-based device can also be used for separation of multiple types of nanoparticles [143] (Fig. 15e). Collins et al. [144] reported separation of particles using virtual deterministic lateral displacement (vDLD) technique where IDTs were placed underneath the microfluidic channel so that electrodes were in direct contact with fluid (Fig. 15f). Using acoustic radiation force and dielectrophoretic force, they were able to separate 500 nm and 300 nm particles with a 50 MHz SAW device. In a subsequent study, Collin et al. [145] developed a traveling SAW-based device for manipulating nanoparticles where they used the microstreaming, generated due to traveling SAWs, to separate nanoparticles based on size. Wu et al. [146] reported successful separation of exosome from whole blood. They have developed an integrated SAW platform combining two modules: one for removing WBCs, RBCs and platelets from blood, and another for extracellular vesicles. In a recent study, Cogal et al. [147] reported regulation of catalytic micromotor speed using SAW. They carried out the experiment in a 96 MHz frequency standing SAW device with SAW power kept at 3 dBm. The secondary Bjerknes force arising due the interaction of acoustic waves and O_2 bubbles, generated via catalytic decomposition of H_2O_2, determines the micromotor speed; by controlling SAW power and frequency, precise control of micromotor motion can be achieved. With these studies, it is clear that SAW devices provide excellent platforms for manipulating cells and particles and thereby show potential in real-world lab-on-chip biosensing applications.

5.5. Fluid mixing

Fluid mixing at microscale is an important step required in many lab-on-a-chip biosensing applications as it helps in reducing the incubation time in biomarker detection. As microscale flows are laminar in nature, mixing ordinarily occurs quite slowly via diffusion. Fortunately, surface acoustic waves have been able to significantly improve mixing rates. Tseng et al. [148] used 35 V (peak to peak) in a 9.6 MHz frequency SAW device to show fluid mixing in a microchannel using SAWs. They used fluorescent dye (Rhodamine B) for visualization and observed significant mixing due to acoustic fluid interactions. Frommelt et al. [149] demonstrated efficient fluid mixing with a SAW mixer chip where a pair of tapered IDTs (TIDTs) were used generate a narrow SAW beam which caused significant acoustic streaming (Fig. 16a). The SAW amplitude and frequency were found to be the parameters that tune the mixing speed. Shilton et al. [150] used 128° rotated Y-cut X-propagating lithium niobate ($LiNbO_3$) medium to generate SAWs and focused them into a droplet via concentric single-phase unidirectional transducers (SPUDTs) to study the fluid mixing (Fig. 16b). Their study showed that focused SPUDTs can cause rapid fluid mixing due to micro acoustic streaming. Liu et al. [151] reported an integrated system of metal-enhanced fluorescence with SAW for rapid detection of cancer biomarkers. In that study, SAW was used to enhance microscale mixing of antigen with antibodies. They used a 79 MHz $LiNbO_3$ SAW device where SAW power was kept at 0 dBm for 10 min and it was observed that the SAW-driven mixing was able to reduce the incubation time from 60 min to about 5 min (Fig. 16c). With these studies, it is clear that SAW-generated acoustic streaming improves microscale mixing within a fluid and can be tuned by adjusting IDT design, SAW amplitude, and SAW power.

5.6. Immunosensors

The highly specific binding of antibodies to antigens is the basis of immunosensors. One of the two is bound on the surface of the sensor so that it can detect the other which is dissolved in the testing solution. SAW sensors employed in this setup detect the mass change at the surface associated with the binding reaction. An extensive range of antigens can be detected and measured by immunosensors: hormones, drugs, bacteria, and even environmental pollutants such as pesticides [124,152]. The first attempt at using a SAW device for the detection of an antigen by an immobilized antibody was made by Roerder and Bastians [153]. A reference and sensing device, fabricated on ST-X quartz, was placed in an oscillator circuit, where the frequency difference was monitored as a function of the amount of antigen bound to the surface. Detection of human IgG was successful, however, future work needed to be done to address the poor sensitivity and the inability to detect small molecules. In subsequent years, other research groups made improvements to this version. Welsch, Klein et al. employed the first immunosensor that

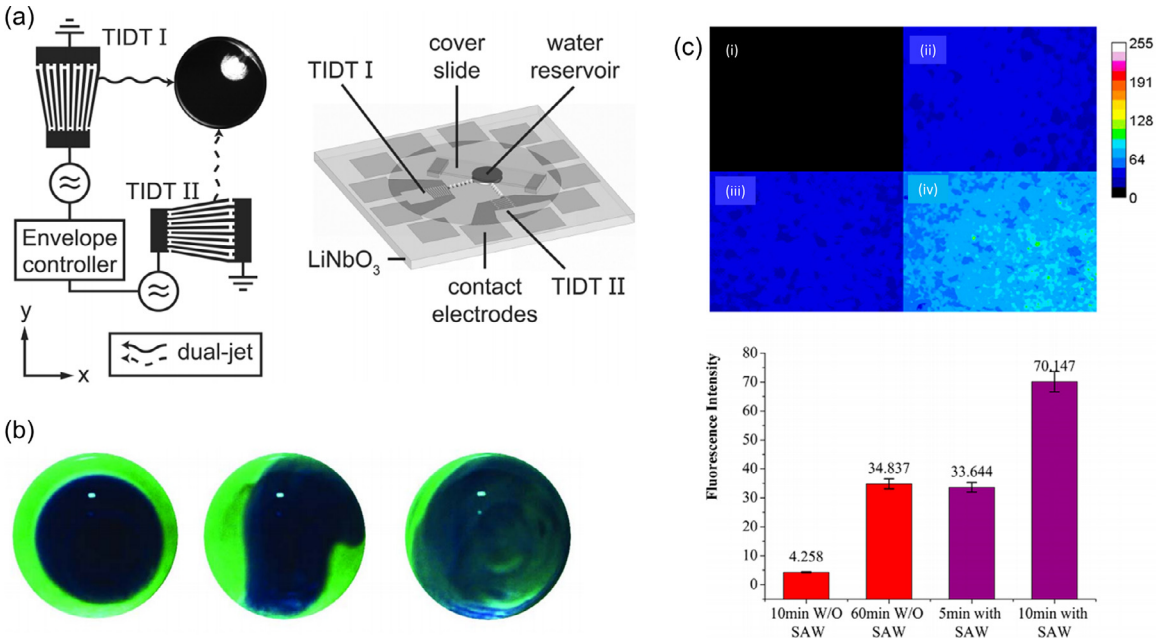

Fig. 16. (a) A SAW mixer chip with TIDTs for generating narrow SAW beam used for fluid mixing in a droplet [149], (b) SAW-induced rapid mixing of water (dark) and glycerin (light) using SPUDT designs [150], and (c) Tuning the mixing effect with SAWs. Chip (i) was treated without SAW for 10 min, (ii) was treated without SAW for 60 min, (iii) was treated with SAW for 5 min at 0 dBm, and (iv) was treated with SAW for 10 min at 0 dBm [151]. Reproduced with permission.

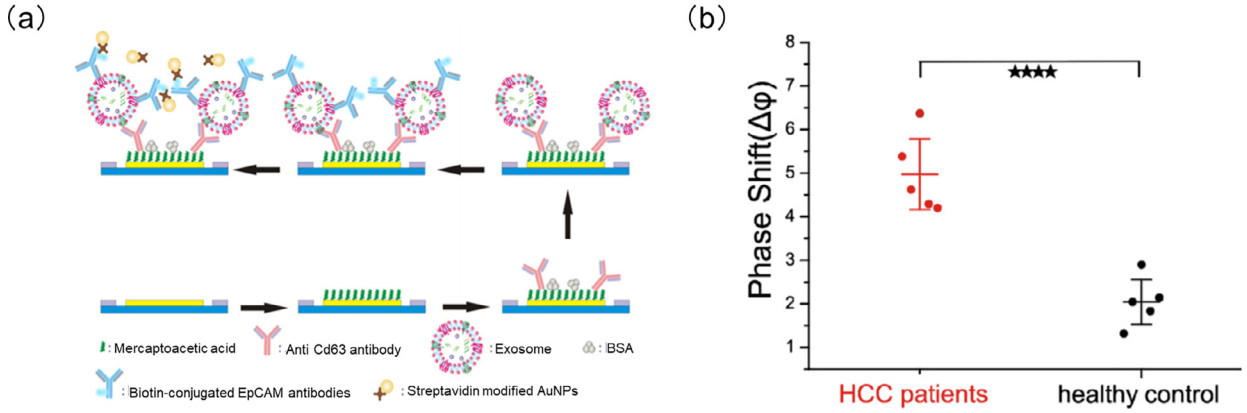

Fig. 17. (a) Schematic of exosome detection process by a double antibody sandwich method and AuNP amplification [157], (b) SAW sensor response to exosomes from hepatocellular carcinoma cancer (HCC) patients and healthy people [157]. Reproduced with permission.

utilized SH-SAWs on a $LiTaO_3$ substrate [154]. By immobilizing amide-coupled polyclonal antibodies, an approach to quantify Escherichia coli L-asparaginase was developed by Yao *et al.* The accuracy and precision are validated at 10 nM concentration of L-asparaginase, which is suitable for quality control in pharmaceutical conditions [155]. Metal nanoparticles have recently been studied as an option to improve the limit of detection. Li *et al.*, using gold chloride trihydrate, synthesized 10–16 nm gold nanoparticles (AuNP) and deposited them on an ST quartz-based Love wave sensor. The addition of gold nanoparticles amplified the mass loading effect for detecting carcinoembryonic antigen, which successfully reduced the limit of detection from 9.4 ng/mL to 37 pg/mL [156]. Similarly, Wang et al. quantified the concentration of exosome using a AuNP-amplified SAW sensor [157]. A Au-S bond was generated by dropping mercaptoacetic acid on the SAW surface in order to immobilize anti-CD63 antibody. The CD63 membrane protein could then be recognized by immobilized antibody, and the quantification process is complete using a secondary antibody followed by assembling AuNP-labeled streptavidin (Fig. 17a) [157]. The AuNP-amplified signal allows the sensor to quantify exosomes down to 1100 particles/mL concentration, which is a hundred times better than without AuNP amplification [157]. The sensor also showed good specificity in detecting exosomes from plasma samples from cancer patients (Fig. 17b) [157]. Drawbacks of SAW biosensors are nonspecific binding, which causes degradation of the test signal, and the difficulty in detecting small molecular weight molecules directly; low molecular weight analytes do not produce sufficient change in mass at the surface [158].

5.7. *DNA sensing*

The hybridization of complementary single stranded DNA (ssDNA) with immobilized ssDNA can be detected with piezoelectric devices. In 2005, researchers developed a SH-SAW sensor on $LiTaO_3$, to detect 15-mer oligonucleotide DNA in liquid solutions by means of the complementary DNA hybridization mechanism [159]. The sensor consisted of a dual delay line device (sensing channel and reference channel) with the probe DNA immobilized on an Au layer deposited on the SAW delay lines. Hybridization between the probe and target resulted in a shift in the oscillation frequency between the reference and the sensing

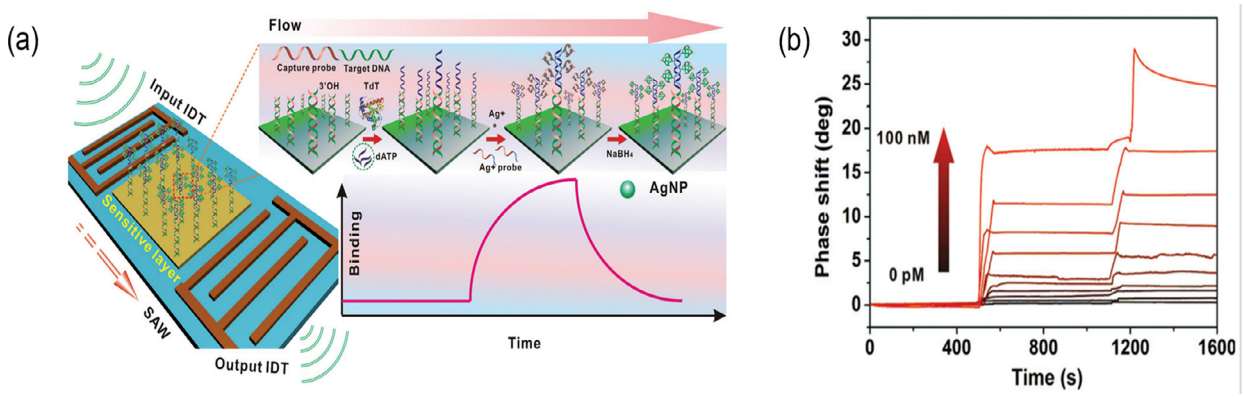

Fig. 18. (a) Schematic of a silver-nanoparticle-amplified DNA sensor, (b) Sensor response to target DNA with a series of concentrations: 0, 2, 5, 10, 50, 100, 500, 2000, 100000 pM [161]. Reproduced with permission.

channels. Outcome from experiments yielded a maximum sensitivity of 155 ng/ml/Hz. Zerrouki et al. used a dual delay-line SAW sensor based on $LiTaO_3$ to detect the frequency responses with respect to the hybridization and grafting of synthesized oligonucleotides to its natural DNA pair [160]. Zhang et al. [161] developed a Love wave DNA sensor used for sequence-specific DNA detection to lower the detection limit of target DNA. The sensor was functionalized with deoxynucleoside transferase which serves as a DNA capture probe and implemented with synthesized silver nanoparticles to amplify the phase shift (Fig. 18a). The detection limit using this method was improved by 3 orders of magnitude to 0.8 pM [161] (Fig. 18b). Other researchers have reported discrimination of DNA mismatches with SAW sensors. Mazouz et al. used a 104 MHz leaky-SAW sensor to detect single base mismatches in synthetic oligonucleotides and single-nucleotide polymorphisms [162]. Gronewold et al. used a Love-wave-based SAW sensor to detect individual point mutations in the cancer gene fragment human BRCA1 [163]. Similarly, Liu et al. proposed a graphene oxide modified SAW sensor for CYP2D6*10 mutation [164]. The diagnostic ability in clinical samples is proven with high sensitivity and specificity [164].

6. Issues in biosensing applications: biofouling

Current biosensors aim to enhance the practicability so as to conduct faster experiments, obtain real-time results, and perform point-of-care tests that have the potential to benefit medical science and public health with expedited diagnostic processes, lower costs, and possibly better accuracy [165]. However, there are many distinct shortcomings for some of the current most popular biosensing methods. Current popular biosensing assays include western blotting, microscopy, immunofluorescence assays, enzyme-linked immunosorbent assays (ELISA), polymerase chain reaction (PCR), and surface plasmon resonance (SPR) [166]. Common challenges that need to be tackled include complications in biomarker isolation, lengthy sample preparation and experimental procedures, false positive and negative determinations, low signal intensity, low sensitivity, and increase in biofouling due to the biological complexities in the sample matrix [167].

One of the most well-known biosensing assays is ELISA, which is used to quantify proteins, viruses, antigens, and antibodies in biological samples [168,169]. The setup of an ELISA assay includes immobilization of the capture antibody to the sensing surface to bind with target analyte antigen, after which the antigen is measured by binding with a biotin and streptavidin-HRP-conjugated detection antibody [169]. ELISA is very sensitive and specific [169] and can quantify an antigen at picogram/ml levels [170]. ELISA can also be applied to different sample types, including blood, serum, plasma, tissue, urine, etc [171,172].

However, for biosensing assays that occur on the sensor surface, such as ELISA and SPR, situations arise in which the capture antibody and sensor surface can be bound to unwanted proteins or complexes causing high background signals that overwhelm the signal from the target analyte. This NSB interference phenomenon weakens the performance of sensors [173,174]. There are many existing methods to reduce NSB protein attachment. A review of literature indicates NSB protein reduction methods are categorized into two major types: passive and active methods [175]. Passive methods mainly focus on preventing attachment of NSB proteins to the sensing surface using a chemical or coating such as bovine serum albumin (BSA) or a hydrophilic boundary layer to prevent protein adsorption [174,175]. Passive methods have existed for decades and are still more prevalent due to their ease of use; active methods, on the other hand, are recent techniques that use transducers to create electromechanical forces that shake off undesired proteins or use fluid flow to wash off NSB proteins from the sensor surface [175]. In this section, we will be mainly concerned with the active method using a SAW transducer device to mitigate biofouling.

SAW devices are direct, label free biosensors that monitor the interaction between a receptor and its target in real time through changes in the properties of the traveling wave (i.e., frequency, velocity, and amplitude). Detection setups that require labels have higher operating costs, longer assay times compared to label-free techniques, and do not allow real time monitoring of the capture event. Moreover, distortion of results can occur due to labels interfering with analyte binding [176]. It appears that label-free biosensors are superior to labeled detection schemes although they do have one inherent drawback. Label-free detection schemes are not able to differentiate between a sensor response caused by the binding of analytes to specific receptors and responses caused by nonspecific material binding to the sensor surface [177]. Currently, most reported sensing systems rely on a buffer solution containing an isolated antigen of interest to circumvent this problem. However, in real point of need (PON) applications. the antigen of interest will be dissolved in a complex biological medium (serum, plasma, blood) which will contain a variety of proteins and other biological molecules [178]. These added species will interfere with the sensor's ability to discern the protein of interest from the background signal by creating an interfering signal. Therefore, it is imperative to reduce or eliminate nonspecific binding to use biosensors in medical diagnostic applications.

6.1. Modification of the substrate surface to decrease nonspecific binding

To operate SAW devices as biosensors, a layer containing the biorecognition element must coat the surface. An ideal surface coating for biosensors should meet the following requirements: (1) an abundance of functional groups to attach biorecognition elements, (2) the retention of biological activity of bio-recognition elements after immobilization, (3) an ultralow fouling background, and (4) long term stability of the functionalized coating [179]. Direct adsorption of the biorecognition element to the substrate is not recommended because of denaturation of the biomolecule and inadequate shielding against nonspecific binding of

additional species contained in the matrix [176]. Therefore, intermediate layers with appropriate surface chemistries can be used to reduce nonspecific binding on non-sensing areas.

Nonspecific binding of proteins is caused by the hydrophobic nature of surfaces, electrostatic interactions between surfaces and partially charged biomolecules, and van der Waals forces [180]. It was shown by Tamura *et al.* that a linear relationship exists between ligand hydrophobicity and the amount of nonspecifically bound proteins [181]. Therefore, a counteractive measure would be to modify the surface so that it is hydrophilic and uncharged. The application of hydrophilic polymers has proven to be effective. Examples of such polymers having low affinity for protein adsorption are poly(ethylene glycol) (PEG) [182], poly (vinyl alcohol) [183], poly(methacrylate) derivatives [184], and poly (acrylamide) [185]. Many of these polymers have to be functionalized to introduce active sites for coupling [186]. The polysaccharide dextran is also commonly used in bioanalytic applications due to its hydrophilic nature and nontoxicity [187]. This hydrogel swells in water to form a three-dimensional matrix for the immobilization of proteins. The use of a three dimensional matrix to immobilize recognition elements has advantages over their immobilization on a two dimensional surface: more binding sites are provided and the environment is more conducive to preservation of the recognition element [188]. The major drawback of these techniques is the elaborate chemistry required, which makes them expensive to implement [189]. Another common technique to reduce nonspecific adsorption is to expose the antibody-coated substrates to other adhesive proteins which block nonspecific adsorption sites [190]. For example, blocking proteins such as BSA or casein are adsorbed on bare regions of the substrate to block other proteins from adhering.

6.2. TSM resonator utilized to remove nonspecifically bound proteins

The efficacy of removing non-specifically bound proteins from a sensing surface with generated acoustic waves was shown using a TSM resonator [191]. The mechanism by which nonspecifically bound proteins may be removed with a TSM resonator is the induction of mechanical stress on proteins via shear wave penetration, which reduces the activation energy of desorption and promotes their removal. For this method to be effective, the film thickness of the sensing system attached to the substrate surface must be within the wave penetration decay length given in Meyer's experiment [191]. Determination of nonspecifically bound protein removal was done by measuring the fluorescent intensity of tagged molecules before, during, and after the device operation at different input power levels. Arrays of 20 × 20 μm squares were used to compute the average signal, background, signal to background and standard deviation values; hence, fluorescent intensity from the sensing squares represents the signal and fluorescent intensity from the non-sensing areas represents the background. At low input power (i.e. 3.5 W) significant removal of nonspecifically bound proteins is indicated by the reduction in fluorescent intensity in both the sensing and non-sensing regions, particularly the non-sensing areas because of the marked increase in the signal to noise ratio. The authors also showed that substantial removal of nonspecifically bound proteins from the sensing area can occur by increasing the input power (14 W and 24.7 W). Not only was nonspecific binding in the sensing area reduced but sensing film integrity was also maintained [191].

6.3. SAWs utilized to remove nonspecifically bound proteins

Acoustic streaming phenomenon, which results from the fluid motion induced by high-intensity sound waves, can be used to remove these nonspecifically bound proteins to allow more accurate measurements and possibly even reuse of these devices. When Rayleigh waves propagate in the piezoelectric device in contact with a fluid, the transfer of momentum into the fluid domain leads to longitudinal wave propagation, giving rise to the phenomenon of acoustic streaming [192]. The SAW-induced acoustic streaming has the potential to detach and remove the non-specifically bound (NSB) proteins from the device surface, as has been shown experimentally [193].

Based on this acoustic streaming principle, Cular et al. showed that SAWs generated on 128° YX $LiNbO_3$ can remove nonspecifically bound proteins from the surface of a sensor. Similar to the experiments conducted by Meyer et al., differentiation between the sensing and non-sensing regions was achieved by inserting a micropattern of 40 × 40 μm squares in the delay path of the SAW sensor via photolithography. To show removal of nonspecifically bound proteins, an antibody, goat anti-mouse IgG, was covalently attached to the surface within the square patterns and specifically bound to the fluorescently-labeled antigen, mouse anti-rabbit IgG. This area constituted the sensing region. The area surrounding the micro pattern array, passivated with unlabeled BSA, was the non-sensing region. Additional fluorescently-labeled BSA, not used as a blocking agent, was applied all over the sensor surface. Acoustic excitation of the delay path significantly decreased the fluorescent intensity of BSA and the antigen in the non-sensing region and BSA in the sensing region while only slightly decreasing the fluorescent intensity of the antigen in the sensing region. The results also showed that, as the RF input power to the device was increased, the amount of material removed increased. Subsequent experiments conducted by the authors verified that the proteins being removed were indeed nonspecifically bound to the surface. To summarize, the authors were able to show that the acoustic cleaning approach did not damage the antibody receptor film or reduce its capacity to bind an antigen. Even though it was demonstrated that SAWs could remove nonspecifically-bound proteins, the mechanism by which this occurs could not be elucidated. In addition, the Rayleigh waves generated on the substrate in this work are not suitable for liquid sensing due to the propagation of compressional waves into the liquid medium. Therefore, to utilize surface cleaning with acoustic waves in biosensing applications, substrates supporting SH-SAWs as well as waves with a shear vertical component (i.e., $LiTaO_3$ and LGX) must be used. This would open up the possibility of simultaneous removal of nonspecifically-bound proteins and sensing on the same device [99]. Not only is removal and sensing possible with these substrates but the protein removed can be quantified by measuring the attenuation and phase shift of the SH-SAW mode. This is not possible with Rayleigh wave devices due to the damping of the waves by liquid loading.

NSB removal and biomarker sensing could also be simultaneously achieved by combining removal with a different sensing modality, such as the detection of a fluorescence signal for biomarker quantification. Recently, SAW streaming has shown potential in the removal of NSB proteins. Liu *et al.* have attached NSB proteins as well as the carcinoembryonic capture antibody (Fitzgerald, 10-C10E) to the sensor surface made from 128° rotated Y-cut X-propagation $LiNbO_3$, and coated in 50 nm silver nanocubes as shown in Fig. 19a. [151]. In this case, the fluorescent dye Alexa-488 was conjugated to the antibody and the resulting fluorescent intensity was measured and used as a detection signal. The silver nanocubes were used to enhance the fluorescence intensity due to surface plasmon resonance effect. Reduction of fluorescence intensity is observed with time at 0 dBm power applied to the sensing surface, indicating removal of the carcinoembryonic capture antibody via the streaming induced by the Rayleigh waves (Fig. 19b). This opens up the possibility of integrating SAW streaming and fluorescence intensity to quantify low-concentration analytes directly from complex matrices such as human plasma, blood or urine. With plasmonic enhancement of the fluorescent signal combined with acoustic streaming, low ng/ml limits of detection of analyte were achieved. The momentum from SAW streaming disrupts the bound between NSB proteins and the functionalized surface and removes them to the ambient environment, often phosphate-buffered saline, where the analyte can still be attached under SAW streaming as shown in Fig 19c. The background noise from NSB proteins can thus be reduced and the detection limit lowered [151]. These results hold great potential in future assays, where SAW sensors can serve as a precise, reliable, and portable biosensing platforms for PON use.

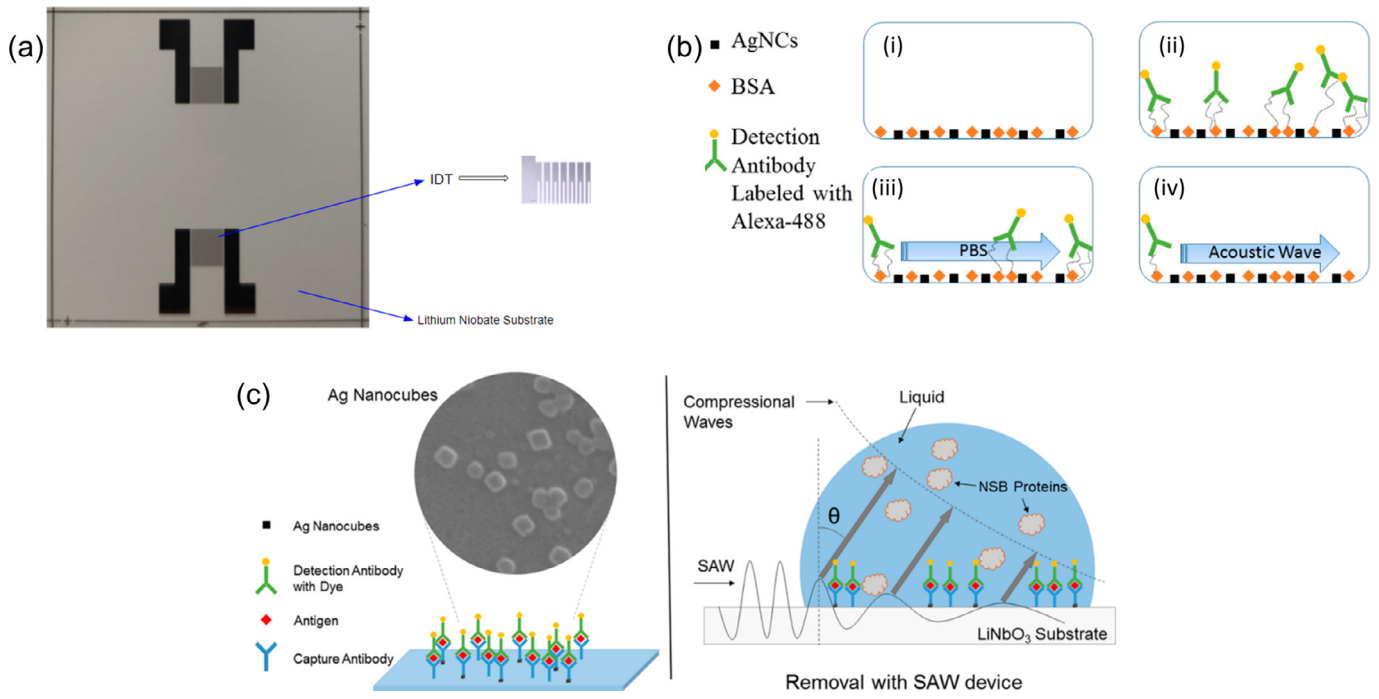

Fig. 19. (a) Image of $LiNbO_3$-based SAW sensor, two IDTs are symmetrically lithographed at either side. (b) Illustration of the NSB protein removal process (i) the surface was functionalized with silver nanocubes and blocked with BSA, (ii) the fluorescently-labeled CEA detection antibody was added and attached to nonspecifically-bound proteins (iii) the surface was rinsed with PBS, removing some but not all detection antibody bound to the NSB proteins, and (iv) efficient removal was done using acoustic streaming. (c) Schematics showing combinations of SAW to remove NSB proteins combined with plasmonic enhancement of the fluorescent signal to quantify the target antigen [151]. Reproduced with permission.

7. Conclusions

SAW biosensors have been widely researched and applied in different sensing applications, including monitoring of cell adhesion and spreading, cell lysis and separation, the detection and quantification of specific proteins and other biomolecules, and the extent of DNA hybridization. In addition to directly sensing the analyte by measuring signal changes based on surface interaction, SAW devices also have potential to further enhance sensitivity and specificity by effectively removing nonspecifically-bound matrix components and by reducing the incubation times. Enhancements to device performance have been achieved by modifying the SAW devices with multi-pair IDTs, microfluidic control, waveguide layers, sensing layers, and microcavities. SAW biosensors have several advantages over traditional bioassays in their fast responsiveness, small size, and high sensitivity. With these benefits, SAW devices show great promise in developing portable low-cost biosensors.

Declaration of Competing Interest

There is no Conflict of Interest to declare.

Acknowledgments

This work was funded by a Strategic Investment Pool grant from University of South Florida and the National Science Foundation (Grant no. IIP-1640668). Pradipta Kr. Das gratefully acknowledges a University of South Florida Presidential Fellowship.

References

[1] D.S. Ballantine Jr, R.M. White, S.J. Martin, A.J. Ricco, E.T. Zellers, G.C. Frye, et al., Acoustic Wave Sensors: Theory, Design and Physico-Chemical Applications, Elsevier, 1996.
[2] A.F. Collings, F. Caruso, Biosensors 60 (1997) 1397.
[3] R.L. Bunde, E.J. Jarvi, J.J. Rosentreter, Piezoelectric quartz crystal biosensors, Talanta 46 (1998) 1223–1236.
[4] D.A. Giljohann, C.A. Mirkin, Drivers of biodiagnostic development, Nature 462 (2009) 461–464.
[5] T. Nomura, M. Okuhara, Frequency shifts of piezoelectric quartz crystals immersed in organic liquids, Anal. Chim. Acta 142 (1982) 281–284.
[6] R.M. White, F.W. Voltmer, Direct piezoelectric coupling to surface elastic waves, Appl. Phys. Lett. 7 (1965) 314–316.
[7] A.J. Ricco, S.J. Martin, T.M. Niemczyk, G.C. Frye, Liquid-Phase Sensors Based on Acoustic Plate Mode Devices, Chemical Sensors and Microinstrumentation, American Chemical Society1989, pp. 191-207.
[8] J.W. Grate, S.W. Wenzel, R.M. White, Flexural plate wave devices for chemical analysis, Anal. Chem. 63 (1991) 1552–1561.
[9] M. Hoummady, A. Campitelli, W. Wlodarski, Acoustic wave sensors: design, sensing mechanisms and applications, Smart Mater. Struct. 6 (1997) 647–657.
[10] S. Li, V.R. Bhethanabotla, Design of a portable orthogonal surface acoustic wave sensor system for simultaneous sensing and removal of nonspecifically bound proteins, Sensors 19 (2019) 3876.
[11] J. Curie, P. Curie, Développement par compression de l'électricité polaire dans les cristaux hémièdres à faces inclinées, Bull. Minéral. 3 (1880) 90–93.
[12] N.R. Skov, P. Sehgal, B.J. Kirby, H. Bruus, Three-dimensional numerical modeling of surface-acoustic-wave devices: acoustophoresis of micro- and nanoparticles including streaming, Phys. Rev. Appl. 12 (2019) 044028.
[13] J.-C. Hsu, C.-L. Chao, Full-wave modeling of micro-acoustofluidic devices driven by standing surface acoustic waves for microparticle acoustophoresis, J. Appl. Phys. 128 (2020) 124502.
[14] Z. Ni, C. Yin, G. Xu, L. Xie, J. Huang, S. Liu, et al., Modelling of SAW-PDMS acoustofluidics: physical fields and particle motions influenced by different descriptions of the PDMS domain, Lab Chip 19 (2019) 2728–2740.
[15] S.K.R.S. Sankaranarayanan, V.R. Bhethanabotla, Design of efficient focused surface acoustic wave devices for potential microfluidic applications, J. Appl. Phys. 103 (2008) 064518.
[16] S. Li, S.K.R.S. Sankaranarayanan, C. Fan, Y. Su, V.R. Bhethanabotla, Achieving lower insertion loss and higher sensitivity in a SAW biosensor via optimization of waveguide and microcavity structures, IEEE Sens. J. 17 (2017) 1608–1616.
[17] M. Richardson, S.K.R.S. Sankaranarayanan, V.R. Bhethanabotla, Low insertion loss and highly sensitive SH-SAW sensors based on 36° YX $LiTaO_3$ through the incorporation of filled microcavities, IEEE Sens. J. 15 (2015) 787–796.
[18] R. Augustine, F. Sarry, N. Kalarikkal, S. Thomas, L. Badie, D. Rouxel, Surface acoustic wave device with reduced insertion loss by electrospinning P(VDF–TrFE)/ZnO nanocomposites, Nano-Micro Lett. 8 (2016) 282–290.
[19] E. Gizeli, Design considerations for the acoustic waveguide biosensor, Smart Mater. Struct. 6 (1997) 700.
[20] R.H. Parmenter, The acousto-electric effect, Phys. Rev. 89 (1953) 990.
[21] C.E. Bradley, Acoustic streaming field structure: The influence of the radiator, J. Acoust. Soc. Am. 100 (1996) 1399–1408.

[22] W.L. Nyborg, Acoustic streaming due to attenuated plane waves, J. Acoust. Soc. Am. 25 (1953) 68–75.
[23] P.K. Das, A.D. Snider, V.R. Bhethanabotla, Acoustic streaming in second-order fluids, Phys. Fluids 32 (2020) 123103.
[24] N. Nama, T.J. Huang, F. Costanzo, Acoustic streaming: an arbitrary Lagrangian–Eulerian perspective, J. Fluid Mech. 825 (2017) 600–630.
[25] P.K. Das, A.D. Snider, V.R. Bhethanabotla, Acoustothermal heating in surface acoustic wave driven microchannel flow, Phys. Fluids 31 (2019) 106106.
[26] A.Y. Rednikov, S.S. Sadhal, Acoustic/steady streaming from a motionless boundary and related phenomena: generalized treatment of the inner streaming and examples, J. Fluid Mech. 667 (2011) 426–462.
[27] A.Y. Rednikov, N. Riley, S.S. Sadhal, The behaviour of a particle in orthogonal acoustic fields, J. Fluid Mech. 486 (2003) 1–20.
[28] C. Bradley, Acoustic streaming field structure. Part II. Examples that include boundary-driven flow, J. Acoust. Soc. Am. 131 (2012) 13–23.
[29] H. Bruus, Acoustofluidics 7: the acoustic radiation force on small particles, Lab Chip 12 (2012) 1014–1021.
[30] L.V. King, On the acoustic radiation pressure on spheres, Proc. R. Soc. Lond. Ser. A – Math. Phys. Sci. 147 (1934) 212–240.
[31] K. Yosioka, Y. Kawasima, Acoustic radiation pressure on a compressible sphere, Acta Acust. United Acust. 5 (1955) 167–173.
[32] L.P. Gor'kov, On the forces acting on a small particle in an acoustical field in an ideal fluid, Soviet Phys. Doklady 6 (1962) 773.
[33] J.T. Karlsen, P. Augustsson, H. Bruus, Acoustic force density acting on inhomogeneous fluids in acoustic fields, Phys. Rev. Lett. 117 (2016) 114504.
[34] R. Barnkob, N. Nama, L. Ren, T.J. Huang, F. Costanzo, C.J. Kähler, Acoustically driven fluid and particle motion in confined and leaky systems, Phys. Rev. Appl. 9 (2018) 014027.
[35] C. Devendran, T. Albrecht, J. Brenker, T. Alan, A. Neild, The importance of travelling wave components in standing surface acoustic wave (SSAW) systems, Lab Chip 16 (2016) 3756–3766.
[36] V. Bjerknes, Fields of Force, The Columbia university press, 1906.
[37] L.A. Crum, Bjerknes forces on bubbles in a stationary sound field, J. Acoust. Soc. Am. 57 (1975) 1363–1370.
[38] D. Beyssen, L. Le Brizoual, O. Elmazria, P. Alnot, I. Perry, D. Maillet, 6i-2 droplet heating system based on saw/liquid interaction, 2006 IEEE Ultrasonics Symposium, IEEE, 2006, pp. 949–952.
[39] J. Kondoh, N. Shimizu, Y. Matsui, M. Sugimoto, S. Shiokawa, Development of temperature-control system for liquid droplet using surface acoustic wave devices, Sens. Actuators A 149 (2009) 292–297.
[40] J. Kondoh, N. Shimizu, Y. Matsui, M. Sugimoto, S. Shiokawa, Temperature-control system for small droplet using surface acoustic wave device, SENSORS, 2005 IEEE, Irvine, CA, IEEE, 2005, pp. 727–730.
[41] R.J. Shilton, V. Mattoli, M. Travagliati, M. Agostini, A. Desii, F. Beltram, et al., Rapid and controllable digital microfluidic heating by surface acoustic waves, Adv. Funct. Mater. 25 (2015) 5895–5901.
[42] L. Rayleigh, On waves propagated along the plane surface of an elastic solid, Proc. Lond. Math. Soc. 1 (1885) 4–11.
[43] L. Lamanna, F. Rizzi, M. Bianco, M. Agostini, M. Cecchini, M.D. Vittorio, et al., Photoresponse of the AlN-based SAW device on polymeric and silicon substrates, IEEE Sens. J. (2020) 1-.
[44] W.P. Jakubik, Surface acoustic wave-based gas sensors, Thin Solid Films 520 (2011) 986–993.
[45] B. Liu, X. Chen, H. Cai, M.Mohammad Ali, X. Tian, L. Tao, et al., Surface acoustic wave devices for sensor applications, J. Semicond. 37 (2016) 021001.
[46] P.V. Wright, A review of SAW resonator filter technology, IEEE 1992 Ultrasonics Symposium Proceedings, 1992, pp. 29–38.
[47] G.S. Calabrese, H. Wohltjen, M.K. Roy, A study of SAW delay line behavior in liquids, IEEE 1986 Ultrasonics Symposium, 1986, pp. 607–610.
[48] F.S. Hickernell, Shear horizontal BG surface acoustic waves on piezoelectrics: a historical note, IEEE Trans. Ultrason. Ferroelectr. Freq. Control 52 (2005) 809–811.
[49] J.L. Bleustein, A new surface wave in piezoelectric materials, Appl. Phys. Lett. 13 (1968) 412–413.
[50] H.S. Paul, K. Renganathan, Free vibrations of a pyroelectric layer of hexagonal (6 mm) class, J. Acoust. Soc. Am. 78 (1985) 395–397.
[51] Y. Ota, K. Nakamura, H. Shimizu, Piezoelectric surface shear wave, Technical Group on Ultrasonics of IECE of Japan, Japan, 1969.
[52] T.B. Pollard, T.D. Kenny, J.F. Vetelino, M.P.d. Cunha, Pure SH-SAW propagation, transduction and measurements on KNbO/sub 3, IEEE Trans. Ultrason. Ferroelectr. Freq. Control 53 (2006) 199–208.
[53] E. Berkenpas, S. Bitla, P. Millard, M.P.d. Cunha, Pure shear horizontal SAW biosensor on langasite, IEEE Trans. Ultrason. Ferroelectr. Freq. Control 51 (2004) 1404–1411.
[54] C.-T. Feng, C.-J. Cheng, M.Z. Atashbar, PMMA/64° YX-LiNbO 3 guided SH-SAW based immunosensing system, SENSORS, 2011 IEEE, IEEE, 2011, pp. 308–311.
[55] A. Mujahid, F.L. Dickert, Surface acoustic wave (SAW) for chemical sensing applications of recognition layers, Sensors 17 (2017) 2716.
[56] M. Thompson, D.C. Stone, Surface-Launched Acoustic Wave Sensors: Chemical Sensing and Thin-Film Characterization, Wiley-Interscience, 1997.
[57] C.T. Chuang, R.M. White, J.J. Bernstein, A thin-membrane surface-acoustic-wave vapor-sensing device, IEEE Electron Device Lett. 3 (1982) 145–148.
[58] T.M.A. Gronewold, Surface acoustic wave sensors in the bioanalytical field: Recent trends and challenges, Anal. Chim. Acta 603 (2007) 119–128.
[59] A. Pantazis, E. Gizeli, G. Konstantinidis, A high frequency GaN Lamb-wave sensor device, Appl. Phys. Lett. 96 (2010) 194103.
[60] L. Lamanna, F. Rizzi, F. Guido, L. Algieri, S. Marras, V.M. Mastronardi, et al., Flexible and transparent aluminum-nitride-based surface-acoustic-wave device on polymeric polyethylene naphthalate, Adv. Electron. Mater. 5 (2019) 1900095.
[61] I.A. Viktorov, Rayleigh and Lamb Waves: Physical Theory and Applications, Plenum, New York, 1967.
[62] T.I. Browning, M.F. Lewis, R.F. Milsom, Surface Acoustic Waves on Rotated Y-cut LiTaO3, IEEE, pp. 586-9.
[63] K. Nakamura, M. Kazumi, H. Shimizu, SH-type and Rayleigh-type surface waves on rotated Y-Cut $LiTaO_3$, 1977 Ultrasonics Symposium, 1977, pp. 819–822.
[64] T. Moriizumi, Y. Unno, S. Shiokawa, New sensor in liquid using leaky SAW, 1987 Ultrasonics Symposium, IEEE, 1987, pp. 579–582.
[65] R.L. Baer, C.A. Flory, Some limitations on the use of leaky SAW mode sensors in liquids, IEEE 1991 Ultrasonics Symposium, 1, 1991, pp. 279–284.
[66] R.F. Mitchell, Spurious Bulk Wave Signals in Acoustic Surface Wave Devices, IEEE, pp. 313-20.
[67] E. Gizelli, A.C. Stevenson, N.J. Goddard, C.R. Lowe, Surface skimming bulk waves: a novel approach to acoustic biosensors, 1991 International Conference on Solid-State Sensors and Actuators, IEEE, 1991, pp. 690–692.
[68] C. Campbell, Surface Acoustic Wave Devices and Their Signal Processing Applications, Elsevier, 2012.
[69] E. Gizeli, A.C. Stevenson, N.J. Goddard, C.R. Lowe, A novel Love-plate acoustic sensor utilizing polymer overlayers, IEEE Trans. Ultrason. Ferroelectr. Freq. Control 39 (1992) 657–659.
[70] B.A. Auld, B.H. Yeh, Theory of surface skimming SH wave guidance by a corrugated surface, 1979 Ultrasonics Symposium, IEEE, 1979, pp. 786–790.
[71] C. Campbell, Surface Acoustic Wave Devices for Mobile and Wireless Communications, Four-Volume Set, Academic press, 1998.
[72] K. Kalantar-Zadeh, W. Wlodarski, Y.Y. Chen, B.N. Fry, K. Galatsis, Novel Love mode surface acoustic wave based immunosensors, Sens. Actuators B 91 (2003) 143–147.
[73] D.D. Deobagkar, V. Limaye, S. Sinha, R.D.S. Yadava, Acoustic wave immunosensing of Escherichia coli in water, Sens. Actuators B 104 (2005) 85–89.
[74] M. Gaso, Y. Jiménez, L. Francis, A. Arnau, Love wave biosensors: a review, State Art Biosens. Gen. Asp. (2013) 277–310.
[75] V.S. Chivukula, M.S. Shur, D. Čiplys, Recent advances in application of acoustic, acousto-optic and photoacoustic methods in biology and medicine, Phys. Status Solidi(a) 204 (2007) 3209–3236.
[76] G. Kovacs, G.W. Lubking, M.J. Vellekoop, A. Venema, Love waves for (bio)-chemical sensing in liquids, IEEE 1992 Ultrasonics Symposium Proceedings, IEEE, 1992, pp. 281–285.
[77] M.J. Vellekoop, Acoustic wave sensors and their technology, Ultrasonics 36 (1998) 7–14.
[78] L. Lamanna, F. Rizzi, V.R. Bhethanabotla, M. De Vittorio, GHz AlN-based multiple mode SAW temperature sensor fabricated on PEN substrate, Sens. Actuators A 315 (2020) 112268.
[79] Z. Li, Y. Jones, J. Hossenlopp, R. Cernosek, F. Josse, Analysis of liquid-phase chemical detection using guided shear horizontal-surface acoustic wave sensors, Anal. Chem. 77 (2005) 4595–4603.
[80] W. Wang, S. He, Theoretical analysis on response mechanism of polymer-coated chemical sensor based Love wave in viscoelastic media, Sens. Actuators B 138 (2009) 432–440.
[81] T. Wessa, N. Barić, M. Rapp, H.J. Ache, Polyimide, a new shielding layer for sensor applications, Sens. Actuators B 53 (1998) 63–68.
[82] P. Roach, S. Atherton, N. Doy, G. McHale, M.I. Newton, SU-8 guiding layer for love wave devices, Sensors 7 (2007) 2539–2547.
[83] G. McHale, M.I. Newton, F. Martin, E. Gizeli, K.A. Melzak, Resonant conditions for Love wave guiding layer thickness, Appl. Phys. Lett. 79 (2001) 3542–3543.
[84] F. Josse, F. Bender, R.W. Cernosek, Guided shear horizontal surface acoustic wave sensors for chemical and biochemical detection in liquids, Anal. Chem. 73 (2001) 5937–5944.
[85] J. Du, G.L. Harding, J.A. Ogilvy, P.R. Dencher, M. Lake, A study of Love-wave acoustic sensors, Sens. Actuators A 56 (1996) 211–219.
[86] K.K. Zadeh, A. Trinchi, W. Wlodarski, A. Holland, A novel Love-mode device based on a ZnO/ST-cut quartz crystal structure for sensing applications, Sens. Actuators A 100 (2002) 135–143.
[87] R.-C. Chang, S.-Y. Chu, C.-S. Hong, Y.-T. Chuang, A study of Love wave devices in ZnO/Quartz and ZnO/LiTaO3 structures, Thin Solid Films 498 (2006) 146–151.
[88] F.-m. Zhou, Z. Li, L. Fan, S.-y. Zhang, X.-j. Shui, Experimental study of Love-wave immunosensors based on ZnO/LiTaO3 structures, Ultrasonics 50 (2010) 411–415.
[89] N. Arana, D. Puente, I. Ayerdi, E. Castano, J. Berganzo, SU8 protective layers in liquid operating SAWs, Sens. Actuators B 118 (2006) 374–379.
[90] J.W. Grate, S.J. Martin, R.M. White, Acoustic wave microsensors, Anal. Chem. 65 (1993) 940A–948A.
[91] E. Gizeli, A.C. Stevenson, N.J. Goddard, C.R. Lowe, Acoustic Love plate sensors: comparison with other acoustic devices utilizing surface SH waves, Sens. Actuators B 14 (1993) 638–639.
[92] C. Steinem, A. Janshoff, Piezoelectric Sensors, Springer Science & Business Media, 2007.
[93] M.-I. Rocha-Gaso, C. March-Iborra, Á. Montoya-Baides, A. Arnau-Vives, Surface generated acoustic wave biosensors for the detection of pathogens: A review, Sensors 9 (2009) 5740–5769.
[94] S. Datta, Surface Acoustic Wave Devices, Prentice Hall, 1986.
[95] F. Martin, M.I. Newton, G. McHale, K.A. Melzak, E. Gizeli, Pulse mode shear horizontal-surface acoustic wave (SH-SAW) system for liquid based sensing applications, Biosens. Bioelectron. 19 (2004) 627–632.
[96] O.A. Williams, V. Mortet, M. Daenen, K. Haenen, Nanocrystalline diamond enhanced thickness shear mode resonator, Appl. Phys. Lett. 90 (2007) 063514.

[97] S. Cular, V.R. Bhethanabotla, D.W. Branch, Simultaneous surface manipulation and sensing in a biosensor using a hexagonal SAW device, AIChE Annual Meeting, 2006.
[98] S. Cular, V.R. Bhethanabotla, D.W. Branch, P2I-6 vapor discrimination using a hexagonal surface acoustic wave device, 2006 IEEE Ultrasonics Symposium, 2006, pp. 1794–1796.
[99] R. Singh, S.K.R.S. Sankaranarayanan, V.R. Bhethanabotla, Orthogonal surface acoustic wave device based on langasite for simultaneous biosensing and biofouling removal, Appl. Phys. Lett. 94 (2009) 263503.
[100] R. Singh, S.K.R.S. Sankaranarayanan, V.R. Bhethanabotla, Enhanced surface acoustic wave biosensor performance via delay path modifications in mutually interacting multidirectional transducer configuration: a computational study, Appl. Phys. Lett. 95 (2009) 034101.
[101] S. Cular, S.K.R.S. Sankaranarayanan, V.R. Bhethanabotla, Enhancing effects of microcavities on shear-horizontal surface acoustic wave sensors: A finite element simulation study, Appl. Phys. Lett. 92 (2008) 244104.
[102] R. Singh, Development of three dimensional fluid-structure interaction models for the design of surface acoustic wave devices: application to biosensing and microfluidic actuation, (2009).
[103] L. Qinghui, W. Xuezhong, D. Di, D. Peitao, F. Dapeng, Design of a novel MEMS IDT dual axes surface acoustic wave gyroscope, 2009 4th IEEE International Conference on Nano/Micro Engineered and Molecular Systems, 2009, pp. 889–892.
[104] X. Ding, S.-C.S. Lin, B. Kiraly, H. Yue, S. Li, I.K. Chiang, et al., On-chip manipulation of single microparticles, cells, and organisms using surface acoustic waves, Proc. Natl. Acad. Sci. 109 (2012) 11105–11109.
[105] C.-P. Lee, Y.-P. Hong, M.-T. Shen, C.-C. Tang, D.C. Ling, Y.-F. Chen, et al., Employing graphene acoustoelectric switch by dual surface acoustic wave transducers, Sci. Rep. 9 (2019) 1–9.
[106] S.R. Fang, S.Y. Zhang, Z.F. Lu, SAW focusing by circular-arc interdigital transducers on YZ-LiNbO/sub 3, IEEE Trans. Ultrason. Ferroelectr. Freq. Control 36 (1989) 178–184.
[107] M.M. de Lima Jr, F. Alsina, W. Seidel, P.V. Santos, Focusing of surface-acoustic-wave fields on (100) GaAs surfaces, J. Appl. Phys. 94 (2003) 7848–7855.
[108] T.-T. Wu, H.-T. Tang, Y.-Y. Chen, Frequency response of a focused SAW device based on concentric wave surfaces: simulation and experiment, J. Phys. D Appl. Phys. 38 (2005) 2986.
[109] T.-T. Wu, H.-T. Tang, Y.-Y. Chen, P.-L. Liu, Analysis and design of focused interdigital transducers, IEEE Trans. Ultrason. Ferroelectr. Freq. Control 52 (2005) 1384–1392.
[110] U. Demirci, Picoliter droplets for spinless photoresist deposition, Rev. Sci. Instrum. 76 (2005) 065103.
[111] D.J. Collins, A. Neild, Y. Ai, Highly focused high-frequency travelling surface acoustic waves (SAW) for rapid single-particle sorting, Lab Chip 16 (2016) 471–479.
[112] D.P. Morgan, Surface-wave devices for signal processing, Stud. Electr. Electron. Eng. 19 (1985).
[113] R.F. Humphryes, Acoustic bulk-surface-wave transducer, Electron. Lett. 5 (1969) 175–176.
[114] D.-P. Chen, J. Melngailis, H.A. Haus, Filters based on conversion of surface acoustic waves to bulk plate modes in gratings, 1982 Ultrasonics Symposium, IEEE, 1982, pp. 67–71.
[115] E. Gizeli, C.R. Lowe, M. Liley, H. Vogel, Detection of supported lipid layers with the acoustic Love waveguide device: application to biosensors, Sens. Actuators B 34 (1996) 295–300.
[116] B.A. Auld, Acoustic Fields and Waves in Solids, vol. One and Two, Robert E. Krieger Publishing Company, Malabar, Florida 1990.
[117] D.W. Branch, S.M. Brozik, Low-level detection of a Bacillus anthracis simulant using Love-wave biosensors on 36°YX LiTaO3, Biosens. Bioelectron. 19 (2004) 849–859.
[118] L. Sun, G. Qin, H. Huang, H. Zhou, N. Behdad, W. Zhou, et al., Flexible high-frequency microwave inductors and capacitors integrated on a polyethylene terephthalate substrate, Appl. Phys. Lett. 96 (2010) 013509.
[119] S. Kim, W. Lee, C. Lee, Influence of ZnO buffer layer thickness on electrical and optical properties of GZO thin films deposited on polymer substrates, Mater. Sci. Technol. 23 (2007) 303–306.
[120] Y.C. Lin, M.Z. Chen, C.C. Kuo, W.T. Yen, Electrical and optical properties of ZnO:Al film prepared on polyethersulfone substrate by RF magnetron sputtering, Colloids Surf. A 337 (2009) 52–56.
[121] X. Wang, X. Zeng, D. Huang, X. Zhang, Q. Li, The properties of Al doped ZnO thin films deposited on various substrate materials by RF magnetron sputtering, J. Mater. Sci. Mater. Electron. 23 (2012) 1580–1586.
[122] J.-M. Kim, P. Thiyagarajan, S.-W. Rhee, Deposition of Al-doped ZnO films on polyethylene naphthalate substrate with radio frequency magnetron sputtering, Thin Solid Films 518 (2010) 5860–5865.
[123] M. Akiyama, Y. Morofuji, T. Kamohara, K. Nishikubo, Y. Ooishi, M. Tsubai, et al., Preparation of oriented aluminum nitride thin films on polyimide films and piezoelectric response with high thermal stability and flexibility, Adv. Funct. Mater. 17 (2007) 458–462.
[124] L. Lamanna, F. Rizzi, V.R. Bhethanabotla, M. De Vittorio, Conformable surface acoustic wave biosensor for E-coli fabricated on PEN plastic film, Biosens. Bioelectron. 163 (2020) 112164.
[125] J. Zhou, X. He, H. Jin, W. Wang, B. Feng, S. Dong, et al., Crystalline structure effect on the performance of flexible ZnO/polyimide surface acoustic wave devices, J. Appl. Phys. 114 (2013) 044502.
[126] Y. Ai, C.K. Sanders, B.L. Marrone, Separation of Escherichia coli Bacteria from peripheral blood mononuclear cells using standing surface acoustic waves, Anal. Chem. 85 (2013) 9126–9134.
[127] F. Di Pietrantonio, M. Benetti, D. Cannatà, E. Verona, A. Palla-Papavlu, J.M. Fernández-Pradas, et al., A surface acoustic wave bio-electronic nose for detection of volatile odorant molecules, Biosens. Bioelectron. 67 (2015) 516–523.
[128] C. Wu, L. Du, D. Wang, L. Wang, L. Zhao, P. Wang, A novel surface acoustic wave-based biosensor for highly sensitive functional assays of olfactory receptors, Biochem. Biophys. Res. Commun. 407 (2011) 18–22.
[129] N.H. Hasanuddin, M.H.A. Wahid, M.M. Shahimin, N. Hambali, N.S. Nazir, N.Z. Khairuddin, et al., Design and development of ZnO based gas sensor for fruit ripening detection, MATEC Web of Conferences, EDP Sciences, 2016, p. 01109.
[130] J. Devkota, P.R. Ohodnicki, D.W. Greve, SAW sensors for chemical vapors and gases, Sensors 17 (2017) 801.
[131] T.J. Lyford, P.J. Millard, M.P.d. Cunha, Cell Lysis using surface acoustic wave devices for sensor applications, 2012 IEEE International Ultrasonics Symposium, 2012, pp. 1216–1219.
[132] D. Taller, K. Richards, Z. Slouka, S. Senapati, R. Hill, D.B. Go, et al., On-chip surface acoustic wave lysis and ion-exchange nanomembrane detection of exosomal RNA for pancreatic cancer study and diagnosis, Lab Chip 15 (2015) 1656–1666.
[133] J. Reboud, Y. Bourquin, R. Wilson, G.S. Pall, M. Jiwaji, A.R. Pitt, et al., Shaping acoustic fields as a toolset for microfluidic manipulations in diagnostic technologies, Proc. Natl. Acad. Sci. 109 (2012) 15162–15167.
[134] B. Alberts, A.D. Johnson, J. Lewis, D. Morgan, M. Raff, K. Roberts, et al., Molekularbiologie der Zelle, John Wiley & Sons, 2017.
[135] C. Gao, S. Peng, P. Feng, C. Shuai, Bone biomaterials and interactions with stem cells, Bone Res. 5 (2017) 1–33.
[136] S.A. Hunter, J.R. Cochran, Chapter two - cell-binding assays for determining the affinity of protein–protein interactions: technologies and considerations, in: V.L. Pecoraro (Ed.), Methods in Enzymology, Academic Press, 2016, pp. 21–44.
[137] F. Klumpers, U. Götz, T. Kurtz, C. Herrmann, T.M.A. Gronewold, Conformational changes at protein–protein interaction followed online with an SAW biosensor, Sens. Actuators B 203 (2014) 904–908.
[138] M. Saitakis, A. Dellaporta, E. Gizeli, Measurement of two-dimensional binding constants between cell-bound major histocompatibility complex and immobilized antibodies with an acoustic biosensor, Biophys. J. 95 (2008) 4963–4971.
[139] J. Nam, H. Lim, D. Kim, S. Shin, Separation of platelets from whole blood using standing surface acoustic waves in a microchannel, Lab Chip 11 (2011) 3361–3364.
[140] P. Li, Z. Mao, Z. Peng, L. Zhou, Y. Chen, P.-H. Huang, et al., Acoustic separation of circulating tumor cells, Proc. Natl. Acad. Sci. 112 (2015) 4970.
[141] M. Wu, P.-H. Huang, R. Zhang, Z. Mao, C. Chen, G. Kemeny, et al., Circulating tumor cell phenotyping via high-throughput acoustic separation, Small 16 (2020) 2004438.
[142] S. Li, F. Ma, H. Bachman, C.E. Cameron, X. Zeng, T.J. Huang, Acoustofluidic bacteria separation, J. Micromech. Microeng. 27 (2016) 015031.
[143] M. Wu, Z. Mao, K. Chen, H. Bachman, Y. Chen, J. Rufo, et al., Acoustic separation of nanoparticles in continuous flow, Adv. Funct. Mater. 27 (2017) 1606039.
[144] D.J. Collins, T. Alan, A. Neild, Particle separation using virtual deterministic lateral displacement (vDLD), Lab Chip 14 (2014) 1595–1603.
[145] D.J. Collins, Z. Ma, J. Han, Y. Ai, Continuous micro-vortex-based nanoparticle manipulation via focused surface acoustic waves, Lab Chip 17 (2017) 91–103.
[146] M. Wu, Y. Ouyang, Z. Wang, R. Zhang, P.-H. Huang, C. Chen, et al., Isolation of exosomes from whole blood by integrating acoustics and microfluidics, Proc. Natl. Acad. Sci. 114 (2017) 10584.
[147] G. Celik Cogal, P.K. Das, S. Li, A. Uygun Oksuz, V.R. Bhethanabotla, Unraveling the autonomous motion of polymer-based catalytic micromotors under chemical −acoustic hybrid power, Adv. NanoBiomed. Res. (2020) 2000009 n/a.
[148] W.-K. Tseng, J.-L. Lin, W.-C. Sung, S.-H. Chen, G.-B. Lee, Active micro-mixers using surface acoustic waves on Y-cut 128° LiNbO3, J. Micromech. Microeng. 16 (2006) 539–548.
[149] T. Frommelt, M. Kostur, M. Wenzel-Schäfer, P. Talkner, P. Hänggi, A. Wixforth, Microfluidic mixing via acoustically driven chaotic advection, Phys. Rev. Lett. 100 (2008) 034502.
[150] R. Shilton, M.K. Tan, L.Y. Yeo, J.R. Friend, Particle concentration and mixing in microdrops driven by focused surface acoustic waves, J. Appl. Phys. 104 (2008) 014910.
[151] J. Liu, S. Li, V.R. Bhethanabotla, Integrating metal-enhanced fluorescence and surface acoustic waves for sensitive and rapid quantification of cancer biomarkers from real matrices, ACS Sens. 3 (2018) 222–229.
[152] C.L. Morgan, D.J. Newman, C.P. Price, Immunosensors: technology and opportunities in laboratory medicine, Clin. Chem. 42 (1996) 193–209.
[153] J.E. Roederer, G.J. Bastiaans, Microgravimetric immunoassay with piezoelectric crystals, Anal. Chem. 55 (1983) 2333–2336.
[154] W. Welsch, C. Klein, M. Von Schickfus, S. Hunklinger, Development of a surface acoustic wave immunosensor, Anal. Chem. 68 (1996) 2000–2004.
[155] H. Yao, C.S. Fernández, X. Xu, E. Wynendaele, B. De Spiegeleer, A Surface Acoustic Wave (SAW) biosensor method for functional quantification of E. coli L-asparaginase, Talanta 203 (2019) 9–15.
[156] S. Li, Y. Wan, Y. Su, C. Fan, V.R. Bhethanabotla, Gold nanoparticle-based low limit of detection Love wave biosensor for carcinoembryonic antigens, Biosens. Bioelectron. 95 (2017) 48–54.
[157] C. Wang, C. Wang, D. Jin, Y. Yu, F. Yang, Y. Zhang, et al., AuNP-amplified surface acoustic wave sensor for the quantification of exosomes, ACS Sens. 5 (2020) 362–369.
[158] J.E. Pearson, A. Gill, P. Vadgama, Analytical aspects of biosensors, Ann. Clin. Biochem. 37 (2000) 119–145.
[159] Y. Hur, J. Han, J. Seon, Y.E. Pak, Y. Roh, Development of an SH-SAW sensor for the detection of DNA hybridization, Sens. Actuators A 120 (2005) 462–467.

[160] C. Zerrouki, N. Fourati, R. Lucas, J. Vergnaud, J.-M. Fougnion, R. Zerrouki, et al., Biological investigation using a shear horizontal surface acoustic wave sensor: small "Click generated" DNA hybridization detection, Biosens. Bioelectron. 26 (2010) 1759–1762.
[161] Y. Zhang, F. Yang, Z. Sun, Y.-T. Li, G.-J. Zhang, A surface acoustic wave biosensor synergizing DNA-mediated in situ silver nanoparticle growth for a highly specific and signal-amplified nucleic acid assay, Analyst 142 (2017) 3468–3476.
[162] Z. Mazouz, N. Fourati, C. Zerrouki, A. Ommezine, L. Rebhi, N. Yaakoubi, et al., Discriminating DNA mismatches by electrochemical and gravimetric techniques, Biosens. Bioelectron. 48 (2013) 293–298.
[163] T.M.A. Gronewold, A. Baumgartner, E. Quandt, M. Famulok, Discrimination of single mutations in cancer-related gene fragments with a surface acoustic wave sensor, Anal. Chem. 78 (2006) 4865–4871.
[164] X. Liu, J.-Y. Wang, X.-B. Mao, Y. Ning, G.-J. Zhang, Single-shot analytical assay based on graphene-oxide-modified surface acoustic wave biosensor for detection of single-nucleotide polymorphisms, Anal. Chem. 87 (2015) 9352–9359.
[165] A. Kaushik, M.A. Mujawar, Point of care sensing devices: better care for everyone, Sensors 18 (2018) 4303.
[166] D. Hu, S.R. Fry, J.X. Huang, X. Ding, L. Qiu, Y. Pan, et al., Comparison of surface plasmon resonance, resonant waveguide grating biosensing and enzyme linked immunosorbent assay (ELISA) in the evaluation of a dengue virus immunoassay, Biosensors 3 (2013) 297–311.
[167] R. Mayeux, Biomarkers: potential uses and limitations, NeuroRx 1 (2004) 182–188.
[168] L.-n. Ma, J. Zhang, H.-t. Chen, J.-h. Zhou, Y.-z. Ding, Y.-s. Liu, An overview on ELISA techniques for FMD, Virol. J. 8 (2011) 1–9.
[169] M.F. Clark, R.M. Lister, M. Bar-Joseph, ELISA Techniques, Methods in Enzymology, Elsevier, 1986, pp. 742–766.
[170] E. Macy, M. Kemeny, A. Saxon, Enhanced ELISA: how to measure less than 10 picograms of a specific protein (immunoglobulin) in less than 8 hours, FASEB J. 2 (1988) 3003–3009.
[171] H. Kobori, A. Katsurada, K. Miyata, N. Ohashi, R. Satou, T. Saito, et al., Determination of plasma and urinary angiotensinogen levels in rodents by newly developed ELISA, Am. J. Physiol.-Renal Physiol. 294 (2008) F1257–F1F63.
[172] S. Aydin, A short history, principles, and types of ELISA, and our laboratory experience with peptide/protein analyses using ELISA, Peptides 72 (2015) 4–15.
[173] R.L. Rich, D.G. Myszka, Survey of the 1999 surface plasmon resonance biosensor literature, J. Mol. Recognit. 13 (2000) 388–407.
[174] J. Gibbs, M.E. Kennebunk, Effective blocking procedures, ELISA Techn. Bull. 3 (2001) 1–6.
[175] J.Y. Lichtenberg, Y. Ling, S. Kim, Non-specific adsorption reduction methods in biosensing, Sensors 19 (2019) 2488.
[176] B.E. Rapp, F.J. Gruhl, K. Länge, Biosensors with label-free detection designed for diagnostic applications, Anal. Bioanal. Chem. 398 (2010) 2403–2412.
[177] E. Brynda, M. Houska, A. Brandenburg, A. Wikerstål, Optical biosensors for real-time measurement of analytes in blood plasma, Biosens. Bioelectron. 17 (2002) 665–675.
[178] R. Dahint, F. Bender, F. Morhard, Operation of acoustic plate mode immunosensors in complex biological media, Anal. Chem. 71 (1999) 3150–3156.
[179] H. Vaisocherová, Z. Zhang, W. Yang, Z. Cao, G. Cheng, A.D. Taylor, et al., Functionalizable surface platform with reduced nonspecific protein adsorption from full blood plasma—material selection and protein immobilization optimization, Biosens. Bioelectron. 24 (2009) 1924–1930.
[180] G. Markovic, T. Mutschler, K. Wöllner, G. Gauglitz, Application of surface acoustic waves for optimisation of biocompatibility of carboxymethylated dextran surfaces, Surf. Coat. Technol. 201 (2006) 1282–1288.
[181] T. Tamura, T. Terada, A. Tanaka, A quantitative analysis and chemical approach for the reduction of nonspecific binding proteins on affinity resins, Bioconjug. Chem. 14 (2003) 1222–1230.
[182] N.A. Alcantar, E.S. Aydil, J.N. Israelachvili, Polyethylene glycol–coated biocompatible surfaces, J. Biomed. Mater. Res. 51 (2000) 343–351.
[183] D.R. Miller, N.A. Peppas, Diffusional effects during albumin adsorption on highly swollen poly (vinyl alcohol) hydrogels, Eur. Polym. J. 24 (1988) 611–615.
[184] E. Iwaoka, T. Mori, T. Shimizu, K. Hosoya, A. Tanaka, Improvement of monolithic solid material by utilization of spacer for identification of the target using affinity resins, Bioorg. Med. Chem. Lett. 19 (2009) 1469–1472.
[185] S.D. Bruck, Aspects of three types of hydrogels for biomedical applications, J. Biomed. Mater. Res. 7 (1973) 387–404.
[186] J. Piehler, A. Brecht, K.E. Geckeler, G. Gauglitz, Surface modification for direct immunoprobes, Biosens. Bioelectron. 11 (1996) 579–590.
[187] S. Löfås, B. Johnsson, A novel hydrogel matrix on gold surfaces in surface plasmon resonance sensors for fast and efficient covalent immobilization of ligands, J. Chem. Soc. Chem. Commun. (1990) 1526–1528.
[188] J. Homola, Surface plasmon resonance sensors for detection of chemical and biological species, Chem. Rev. 108 (2008) 462–493.
[189] S. Rupp, M. von Schickfus, S. Hunklinger, H. Eipel, A. Priebe, D. Enders, et al., A shear horizontal surface acoustic wave sensor for the detection of antigen–antibody reactions for medical diagnosis, Sens. Actuators B 134 (2008) 225–229.
[190] S. Herrwerth, T. Rosendahl, C. Feng, J. Fick, W. Eck, M. Himmelhaus, et al., Covalent coupling of antibodies to self-assembled monolayers of carboxy-functionalized poly(ethylene glycol): protein resistance and specific binding of biomolecules †, Langmuir 19 (2003) 1880–1887.
[191] G.D. Meyer, J.M. Moran-Mirabal, D.W. Branch, H.G. Craighead, Nonspecific binding removal from protein microarrays using thickness shear mode resonators, IEEE Sens. J. 6 (2006) 254–261.
[192] S. Shiokawa, Y. Matsui, T. Moriizumi, Experimental study on liquid streaming by SAW, Jpn. J. Appl. Phys. 28 (1989) 126.
[193] S. Cular, D.W. Branch, V.R. Bhethanabotla, G.D. Meyer, H.G. Craighead, Removal of nonspecifically bound proteins on microarrays using surface acoustic waves, IEEE Sens. J. 8 (2008) 314–320.